Deliverable Report

Deliverable No: D2.2

Deliverable Title: Polarization-OAM deterministic transferrer

Grant Agreement number: 255914

Project acronym: PHORBITECH

Project title: A Toolbox for Photon Orbital Angular Momentum Technology

Project website address: www.phorbitech.eu

Name, title and organisation of the scientific representative of deliverable's lead beneficiary (task leader):

Dr. Fabio Sciarrino

Sapienza Università di Roma

Rome, Italy

Deliverable table

Deliverable no.	D2.2
Deliverable name	Polarization-OAM deterministic transferrer
WP no.	2
Lead beneficiary no.	2 (UROM)
Nature	P
Dissemination level	PU
Delivery date from Annex I	Month 12
Actual delivery date	30 September 2011

D2.2) Polarization-OAM deterministic transferrer: *Demonstration of deterministic single-photon polarization-OAM couplers for OAM manipulation, assessment of efficiency. Generation and quantum tomography of polarization-OAM hybrid ququarts.[Excerpt from GA-Annex I DoW]*

This deliverable is composed of two separate items: 1) a prototype of a device that performs a deterministic transfer of a qubit between the polarization and orbital-angular-momentum; 2) the experimental generation of four-dimensional quantum states, or ququarts, encoded in the polarization and orbital angular momentum of a single photon.

1) Device for the deterministic transfer of a qubit between the polarization and orbital-angular-momentum.

This device is based on the following intermediate achievements (both reported in separate scientific publications, which are also included in the present deliverable report):

- In Ref.[1] UNAP achieved real-time control of the retardation of liquid-crystal-based q-plates through an externally applied voltage by exploiting electro-optic effects in liquid crystals. Electro-optic q-plates can be operated as electrically driven converters of photon spin into orbital angular momentum, enabling a variation of the orbital angular momentum probabilities of the output photons over a time scale of milliseconds. This achievement will be also reported at month 18 as part of deliverable D1.4.

- In Ref.[2] UNAP showed that an optical setup based on a polarizing Sagnac interferometer combined with a Dove prism can be used as a convenient general-purpose tool for the generation, detection and sorting of spin-orbit states of light. The working principle of this device has been reported in the classical regime and provides higher sorting efficiency and extinction ratio than usual hologram-fiber combinations, and shows much higher stability and ease of alignment than Mach-Zehnder interferometer setups.

All the previous achievements have hence been combined in a single experimental platform in order to implement a polarization-OAM deterministic transferrer operating in the single-photon regime with high fidelity and high efficiency. The details of the device working principle and resulting performances are given in Ref. [3], also attached to the present report. The device concept and performances have been presented to the Steering Committee during the 1st year meeting (held at ICFO, Barcelona, September 16-17), which could hence assess the quality of the device and approve it for delivering.

In the following pages, we further illustrate the device with some photos.

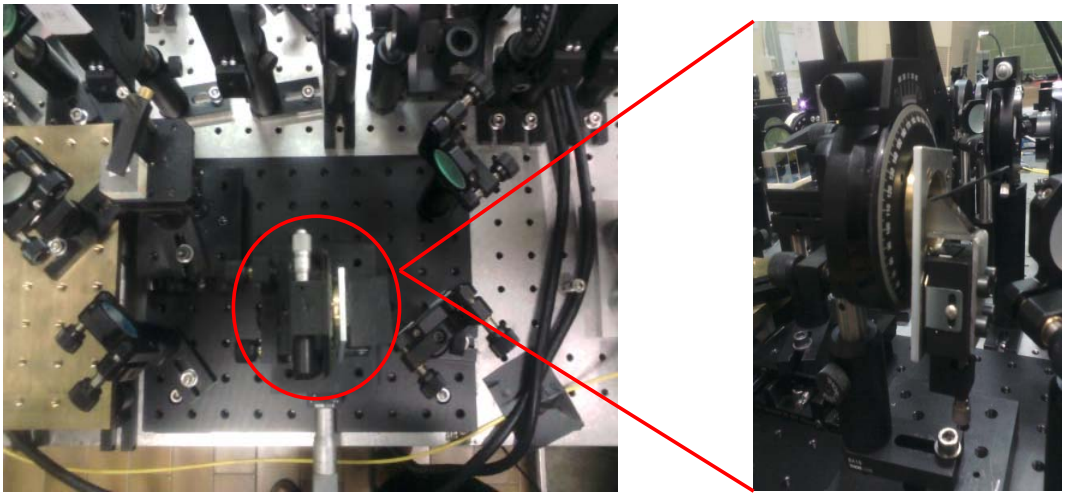

Fig. 1 Pictures of the Sagnac interferometer that is part of the deterministic transferrer device. The red circle indicates the Dove prism (DP) mounting, enlarged on the left side picture.

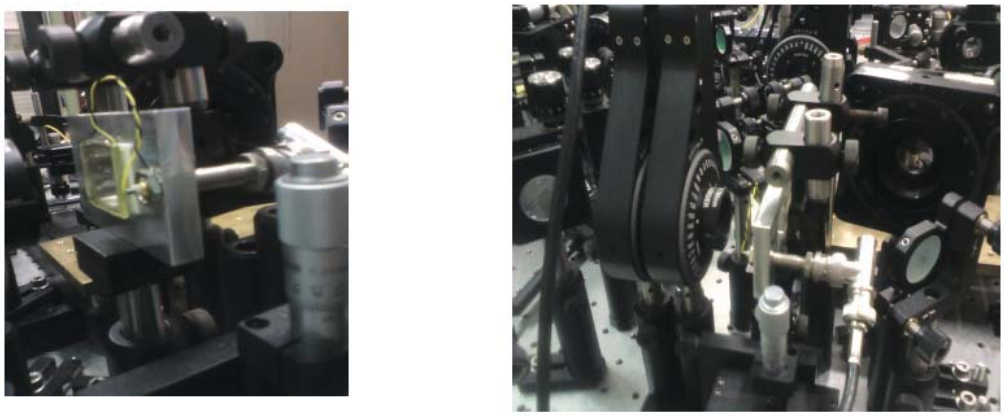

(a) (b)

Fig. 2 (a) Picture of the q-plate mounting. Both the q-plates adopted have been controlled by an electric field, applying a voltage to the liquid crystal. **(b)** Motorized waveplates in order to generate/analyze different states in an automatic way.

2) Experimental generation of four-dimensional quantum states, or ququarts, encoded in the polarization and orbital angular momentum of a single photon.

The adopted technique, based on the q-plate device, allows the ququart to be prepared and measured in all five mutually unbiased bases. The reconstruction of the four-dimensional density matrix through the tomographic procedure for different ququart states has been reported at the beginning of PHORBITECH project in "Experimental generation and characterization of single-photon hybrid ququarts based on polarization and orbital angular momentum encoding" E. Nagali, L. Sansoni, L. Marrucci, E. Santamato, F. Sciarrino , Phys. Rev. A 81, 052317 (2010).

As following step, to demonstrate the manipulation capability of our device, UROM and UNAP reported the first experimental realization of the optimal quantum cloning of four-dimensional quantum states, or ququarts, encoded in the polarization and orbital angular momentum degrees of freedom of photons in Ref. [4]. Optimal quantum cloning is the process of making one or more copies of an arbitrary unknown input quantum state with the highest possible fidelity.

Publications included in this deliverable (see following pages)**:**

[1] “Photon spin-to-orbital angular momentum conversion via an electrically tunable q-plate”, B. Piccirillo, V. D'Ambrosio, S. Slussarenko, L. Marrucci, E. Santamato, Appl. Phys. Lett. **97**, 241104 (2010) [NOTE: this publication will be also reported at month 18 as part of deliverable D1.4]

[2] “The Polarizing Sagnac Interferometer: a tool for light orbital angular momentum sorting and spin-orbit photon processing”, S. Slussarenko, V. D'Ambrosio, B. Piccirillo, L. Marrucci, E. Santamato, Opt. Express **18**, 27205-27216 (2010).

[3] “Deterministic qubit transfer between orbital and spin angular momentum of single photons”, V. D'Ambrosio, E. Nagali, C. Monken, S. Slussarenko, L. Marrucci, and F. Sciarrino, paper submitted to Optics Letters, also published as arXiv:1109.6747.

[4] “Experimental Optimal Cloning of Four-Dimensional Quantum States of Photons”, E. Nagali, D. Giovannini, L. Marrucci, S. Slussarenko, E. Santamato, F. Sciarrino, Phys. Rev. Lett. **105**, 073602 (2010).

Photon spin-to-orbital angular momentum conversion via an electrically tunable *q*-plate

Bruno Piccirillo,[1,a)] Vincenzo D'Ambrosio,[1] Sergei Slussarenko,[1] Lorenzo Marrucci,[1,2] and Enrico Santamato[1]
[1]*Dipartimento di Scienze Fisiche, Università di Napoli "Federico II", Complesso Universitario di Monte S. Angelo, 80126 Napoli, Italy*
[2]*CNR-SPIN, Complesso Universitario di Monte S. Angelo, 80126 Napoli, Italy*

(Received 20 October 2010; accepted 23 November 2010; published online 16 December 2010)

Exploiting electro-optic effects in liquid crystals, we achieved real-time control of the retardation of liquid-crystal-based *q*-plates through an externally applied voltage. Electro-optic *q*-plates can be operated as electrically driven converters of photon spin into orbital angular momentum, enabling a variation of the orbital angular momentum probabilities of the output photons over a time scale of milliseconds. © *2010 American Institute of Physics*. [doi:10.1063/1.3527083]

For years the orbital angular momentum (OAM) of photons has been consigned to a back seat in the study of both classical and quantum optics. This was partly due to the conceptual reason that, in general, the spin and orbital contributions of the electromagnetic angular momentum cannot be considered separately,[1] except within the paraxial approximation. However, even in the small-angle limit, the OAM, due to the dearth of tools suitable for its manipulation, has been used much less than spin angular momentum (SAM). No doubt, the interest for both fundamental and applicative aspects of OAM has kept up with the development of methods and devices for its manipulation. At present, the importance of OAM for quantum optics is mainly due to the fact that it is defined on an infinite-dimensional Hilbert space and, by its own nature, could be suitable for implementing single-photon qudits, which may lead, for example, to simplifying quantum computations[2] and improving quantum cryptography.[3] The most commonly used methods for generating and manipulating the OAM are based on computer generated holograms (CGHs). A recently introduced tool for OAM control is a liquid-crystal-based birefringent plate with retardation δ and optical axis unevenly oriented according to a distribution with topological charge q, after which the name *q*-plate (QP).[4] A QP modifies the angular momentum state of an incident photon by giving to each of its circularly polarized components a finite probability, depending on the retardation δ, of finding the photon in a polarization state with opposite helicity and OAM quantum number l increased or decreased by the amount $\Delta l = 2q$, whether the initial helicity is positive or negative, respectively. In *q*-plates with $q = 1$, the optical axis distribution is cylindrically symmetric around the central defect and the total angular momentum of the incident photons is therefore conserved [SAM-to-OAM conversion (STOC)]. The adoption of such device in quantum optics has recently enabled the observation of two-photon Hong–Ou–Mandel coalescence interference of photons carrying nonzero OAM and the demonstration of the $1 \rightarrow 2$ universal optimal quantum cloning of OAM-encoded qubits and qudits.[5] Besides the topological charge q, a key-feature of a QP is the birefringent retardation since it enables to regulate the probability of switching between l and $l \pm 2q$, i.e., the STOC efficiency, according to the wavelength of the input photons. High efficiencies for generation, manipulation, and detection of OAM states are often desirable, especially when only few photons are available.

In this paper, to achieve a full control of the STOC efficiency, we present an electro-optical *q*-plate (EOQP) whose retardation may be changed through an externally applied voltage. Hitherto, STOC efficiencies exceeding 95% (significantly higher than the efficiencies of the CGHs) were obtained tuning the *q*-plate retardation δ by controlling the material temperature.[6] A thermally tuned QP has been used with a Dove prism inserted into a Sagnac polarizing interferometer in order to generate arbitrary linear combinations of OAM eigenstates with $l = \pm 2$ by manipulating the polarization state of an input linearly polarized TEM_{00} laser beam.[7] The thermal tunability of δ arises from the temperature dependence of the liquid crystal order parameter and ultimately of the intrinsic birefringence of such material. The thermal control of a QP assures an easy-to-made stable retardation at the cost of a very slow time response. This is a limitation whenever the experiment requires a real-time variation of STOC efficiency, for instance, for qudit manipulation or when more wavelengths are involved. Electric-field-based regulation of δ enables one to overcome the time-response limitations imposed by the thermal method and make QPs suitable for more demanding tasks. The working principle of EOQP is based on the well-known property of external static electric or magnetic fields to change the orientation of the liquid-crystal molecular director $\boldsymbol{n}$, representing the local average orientation of liquid crystal molecules.[8] We fabricated and tested two EOQPs with $q = 1$ so that the OAM impressed to converted photons is $l = \pm 2$. These devices have different thicknesses and have been manufactured by different methods. The first was a nominal 20 μm thick film of E7 liquid crystal from Merck Ltd., sandwiched between two indium-tin-oxide (ITO)-coated glass substrates, beforehand coated with a polyimide for planar alignment and circularly rubbed, as described elsewhere.[6] The second EOQP was a nominal 6 μm thick film of E7, sandwiched between two ITO-coated glass substrates, beforehand coated with a polyimide UV-photoaligned for planar topologically charged optical axis distribution. The ITO transparent conductive films work as electrodes for the application of an electric field to the liquid

a)Electronic mail: bruno.piccirillo@na.infn.it.

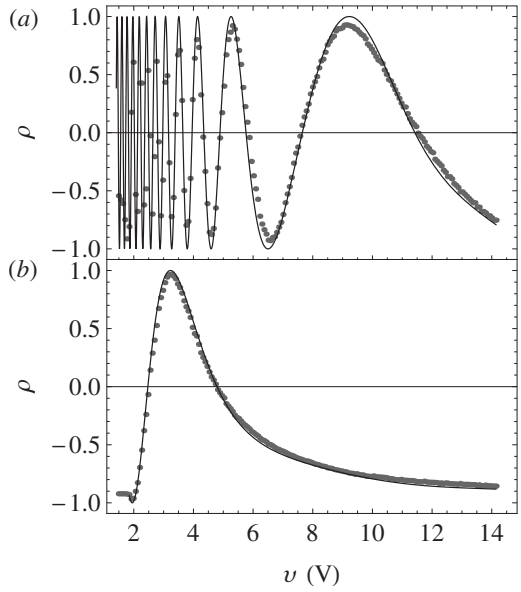

FIG. 1. Measured contrast ratio $\rho(v)=\cos\delta(v)$ reported as function of v for $EOQP_1$ (a) and $EOQP_2$ (b). The continuous lines represent the theoretical behaviors.

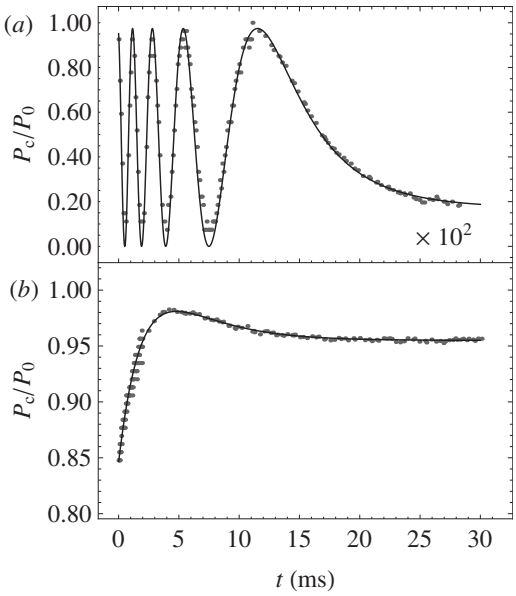

FIG. 3. Time decay of the power of the converted components of the output beam for $EOQP_1$ (a) and $EOQP_2$ (b) after the voltage switch-off. The starting voltages were $v_1=2.8$ V for $EOQP_1$ and $v_2=2.2$ V for $EOQP_2$ so that the dynamics may be approached in the small distortion limit and compared with theory (continuous lines). The time scale in panel (a) is slower by a factor of 100 with respect to panel (b).

crystal. From now on, the former device will be referred to as $EOQP_1$ and the latter as $EOQP_2$. Adopting essentially the same apparatus as that described in Ref. 6 for both the EOQPs, we measured, as a function of the applied voltage, the powers of the converted (P_c) and unconverted (P_u) components of the output beam for an incident $\lambda=532$ nm circularly polarized TEM_{00} laser beam. The temperature of both the EOQPs was maintained stable at 30 °C during measurements. P_u and P_c are expected to depend on the optical retardation δ according to the Malus-like laws,[6] $P_u=P_0\cos^2(\delta/2)$ and $P_c=P_0\sin^2(\delta/2)$, where P_0 is the total output power. In Fig. 1, the contrast ratios $\rho(v)=(P_u-P_c)/(P_u+P_c)=\cos\delta(v)$ are shown for the rubbing-aligned and UV-photoaligned EOQPs, respectively, as functions of the rms values v of the applied 1 kHz ac voltage.[9] The dependence of $\delta(v)$ on the voltage arises from the torque exerted on the liquid crystal molecules by the applied electric field.[8] The behavior of $\delta(v)$ vs v, as deduced from $\rho(v)$, is shown in Fig. 2 for both devices. For $v<v_{th}=1.85\pm0.01$ V, the nematic is undistorted in both the EOQPs and $\delta(0)=\delta_0=2\pi\Delta nL/\lambda+\delta_0^*$, where L stands for the thickness of the cell, $\Delta n=0.23$ is the intrinsic birefringence of the nematic E7 at 30 °C, and δ_0^* is a small constant residual birefringence. For $EOQP_1$, $\delta_0\approx1.7\pi$ and for $EOQP_2$, $\delta_0\approx0.8\pi$. For $v=v_{th}$ there is a discontinuity in the slope $d\delta/dv$. This is peculiar of a second order phase transition between the unperturbed and the distorted conformations at the critical voltage v_{th} (Freédericksz transition).[8] The theory of electro-optical effects in liquid crystals[8] predicts that $v_{th}=\pi\sqrt{k_{11}/\epsilon_0\epsilon_a}$, where $k_{11}=9.2\times10^{-12}$ N (30 °C) is the splay elastic constant of the liquid crystal,[10] ϵ_0 is the vacuum dielectric constant, and $\epsilon_a=14.3$ at 1 kHz at 30 °C.[11] Actually, such expression returns $v_{th}\lesssim1$ V, i.e., half the experimental value. Such disagreement could be ascribed to the underlying simplified assumption of pure splay deformation. However, consistent with the theory, the experimental values of v_{th}, within the experimental uncertainties, turn out to be the same for both EOQPs, which differ from one another in the thickness only. In the limit of high applied voltage, the overall change $\Delta=\delta_0-\delta(\infty)=\delta_0-\delta_0^*=2\pi\Delta nL/\lambda$ is $\Delta\approx56.8$ for $EOQP_1$ and $\Delta\approx6.1$ for $EOQP_2$, yielding $L\approx21$ μm for $EOQP_1$ and $L\approx2.3$ μm for $EOQP_2$, respectively.

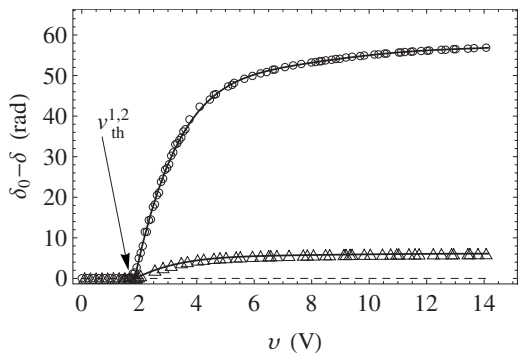

FIG. 2. The optical phase change $\delta(v)$ vs the applied voltage as extracted from the contrast $\rho(v)$ for $EOQP_1$ (○) and $EOQP_2$ (△). The continuous lines correspond to sixth order polynomial curve obtained by fitting the experimental data.

The different thicknesses of the cells are responsible for the different saturation values of $\delta(v)$ and for their different switching-off times. Assuming, for simplicity, that the initial director alignment is homogeneous, the switching-off reorientation in the small distortion limit is expected to decay exponentially in time with a constant $\tau=\gamma_1/k_{11}(L/\pi)^2$, where $\gamma_1=150$ mPa (30 °C) is the rotational viscosity of the liquid crystal.[12] The time behavior of the switching-off P_c signals is consistent with such prediction and the measured decay time constants are $\tau_1=0.931\pm0.002$ s and $\tau_2=(0.80\pm0.01)\times10^{-2}$ s, respectively (Fig. 3). These values are in reasonable agreement with those expected from theory, i.e., $\tau_1^{theor}=0.53$ s and $\tau_2^{theor}=0.62\times10^{-2}$ s. Nevertheless, consistent with the theoretical prediction for τ, $EOQP_2$, due to its reduced thickness, switches off much faster than

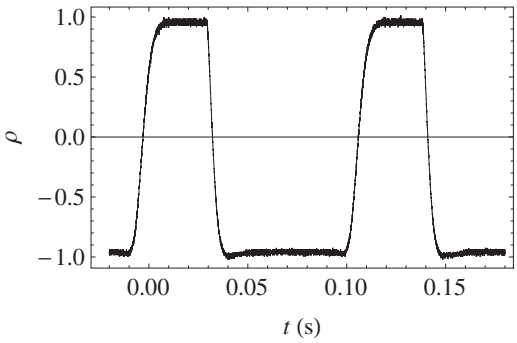

FIG. 4. Time behavior of contrast ratio ρ for on-off switching of the applied voltage (v_{on}=3.2 V) for $EOQP_2$.

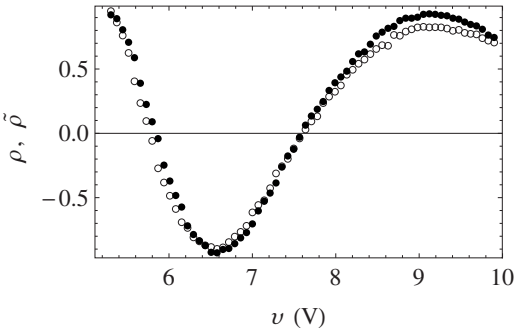

FIG. 5. Contrast ratio vs voltage for the output beam sorted with respect to polarization, $\rho(v)$, (●) and with respect to OAM, $\tilde{\rho}(v)$, (○). Data refer to $EOQP_1$.

$EOQP_1$ and may be used for fast switching between different values of δ, as shown in Fig. 4. Finally, in order to check that the EOQPs actually work as SAM-to-OAM converters, the OAM of the output beam was directly measured adopting a method of sorting between $l=0$ and $l=\pm 2$ based on a polarizing Sagnac interferometer, with a Dove prism inserted along one of its arm, as elsewhere suggested.[7] For $EOQP_1$, the contrast ratio between the OAM components of the output beam was measured as $\tilde{\rho}(v)=(P_0-P_2)/(P_0+P_2)$, where P_0 and P_2 are the powers of the $l=0$ and $l=|2|$ output components, respectively. In Fig. 5, $\tilde{\rho}(v)$ was reported, for comparison, together with $\rho(v)$, as reported in Fig. 1(a), but over a restricted voltage interval (5–10 V). The correlation between the two signals is 99.6%.

In summary we realized an electro-optical SAM-to-OAM converter aimed not only at improving the handiness of classical QPs but also at performing unusual tasks exploiting the capability of EOQPs of managing superpositions of OAM eigenstates with $l=0$, $l=2$, and $l=-2$ in real-time for high-dimensional qudits' manipulation.

We acknowledge the financial support of the FET-Open Program within the Seventh Framework Programme of the European Commission under Grant No. 255914—Phorbitech.

[1]J. D. Jackson, *Classical Electrodynamics* (Wiley, New York, 1989).
[2]A. Muthukrishnan and C. R. Stroud, Jr., Phys. Rev. A **62**, 052309 (2000); B. P. Lanyon, M. Barbieri, M. P. Almeida, T. Jennewein, T. C. Ralph, K. J. Resch, G. J. Pryde, J. L. O'Brien, A. Gilchrist, and A. G. White, Nat. Phys. **5**, 134 (2009).
[3]I. Bregman, D. Aharonov, M. Ben-Or, and H. S. Eisenberg, Phys. Rev. A **77**, 050301 (2008).
[4]L. Marrucci, C. Manzo, and D. Paparo, Phys. Rev. Lett. **96**, 163905 (2006).
[5]E. Nagali, F. Sciarrino, F. D. Martini, L. Marrucci, B. Piccirillo, E. Karimi, and E. Santamato, Phys. Rev. Lett. **103**, 013601 (2009); E. Nagali, L. Sansoni, F. Sciarrino, F. D. Martini, L. Marrucci, B. Piccirillo, E. Karimi, and E. Santamato, Nat. Photonics **3**, 720 (2009); E. Nagali, D. Giovannini, L. Marrucci, E. Santamato, and F. Sciarrino, Phys. Rev. Lett. **105**, 073602 (2010).
[6]E. Karimi, B. Piccirillo, E. Nagali, L. Marrucci, and E. Santamato, Appl. Phys. Lett. **94**, 231124 (2009).
[7]E. Karimi, S. Slussarenko, B. Piccirillo, L. Marrucci, and E. Santamato, Phys. Rev. A **81**, 053813 (2010).
[8]P. G. de Gennes, *The Physics of Liquid Crystals* (Oxford University Press, Oxford, 1974); L. M. Blinov and V. G. Chigrinov, *Electrooptic Effects in Liquid Crystal Materials* (Springer, Berlin, 1996).
[9]An ac rather than a dc voltage is applied to avoid electrochemical degradation (Ref. 8).
[10]H. Hakemi, Mol. Cryst. Liq. Cryst. **287**, 215 (1996).
[11]H.-H. Liu and W. Lee, Appl. Phys. Lett. **97**, 023510 (2010).
[12]Z. Ran, P. Zeng-Hui, L. Yong-Gang, Z. Zhi-Gang, and X. Li, Chin. Phys. B **18**, 4380 (2009).

The Polarizing Sagnac Interferometer: a tool for light orbital angular momentum sorting and spin-orbit photon processing

S. Slussarenko,[1] V. D'Ambrosio,[1] B. Piccirillo,[1,2] L. Marrucci,[1,3] and E. Santamato[1,2,*]

[1]*Dipartimento di Scienze Fisiche, Università di Napoli "Federico II", Complesso Universitario di Monte S. Angelo, 80126 Napoli, Italy*

[2]*CNISM-Consorzio Nazionale Interuniversitario per le Scienze Fisiche della Materia, Napoli, Italy*

[3]*CNR-SPIN, Complesso Universitario di Monte S. Angelo, 80126 Napoli, Italy*

**enrico.santamato@na.infn.it*

Abstract: In this paper we show that an optical setup based on a polarizing Sagnac interferometer combined with a Dove prism can be used as a convenient general-purpose tool for the generation, detection and sorting of spin-orbit states of light. This device can work both in the classical and in the quantum single-photon regime, provides higher sorting efficiency and extinction ratio than usual hologram-fiber combinations, and shows much higher stability and ease of alignment than Mach-Zehnder interferometer setups. To demonstrate the full potential of this setup, we also report some demonstrative experiments of several possible applications of this setup.

OCIS codes: (050.4865) Optical vortices;(270.5585) Quantum information and processing; (120.3180) Interferometry.

References and links

1. M. J. Padgett and J. P. Lesso, "Dove prisms and polarized light," J. Mod. Opt. **46**, 175–179 (1999).
2. G. P. I. Moreno and M. Strojnik, "Polarization transforming properties of dove prisms," Opt. Commun. **220**, 257-268 (2003).
3. I. Moreno, "Jones matrix for image-rotation prisms," Appl. Opt. **43**, 3373-3381 (2004).
4. L. Allen, M. W. Beijersbergen, R. J. C. Spreeuw, and J. P. Woerdman, "Orbital angular momentum of light and the transformation of Laguerre-Gaussian laser modes," Phys. Rev. A **45**, 8185–8189 (1992).
5. L. Allen, S. M. Barnett, and M. J. Padgett, eds., *Optical angular momentum* (Institute of Physics Publishing, Bristol, 2003).
6. G. Molina-Terriza, J. P. Torres, and L. Torner, "Twisted photons," Nat. Phys. **3**, 305–310 (2007).
7. S. Franke-Arnold, L. Allen, and M. Padgett, "Advances in optical angular momentum," Laser Photon. Rev. **2**, 299–313 (2008).
8. A. V. Sergienko, *Quantum Communications and Cryptography* (Taylor & Francis Group, 2006).
9. G. Molina-Terriza, J. P. Torres, and L. Torner, "Management of the angular momentum of light: Preparation of photons in multidimensional vector states of angular momentum," Phys. Rev. Lett. **88**, 013601 (2002).
10. G. Molina-Terriza, A. Vaziri, J. Rehacek, Z. Hradil, and A. Zeilinger, "Triggered qutrits for quantum communication protocols," Phys. Rev. Lett. **92**, 167903 (2004).
11. G. Gibson, J. Courtial, M. J. Padgett, M. Vasnetsov, V. Pasko, S. M. Barnett, and S. Franke-Arnold, "Free-space information transfer using light beams carrying orbital angular momentum," Opt. Express **12**, 5448–5456 (2004).
12. D. Kaszlikowski, P. Gnacinski, M. Zukowski, W. Miklaszewski, and A. Zeilinger, "Violations of local realism by two entangled n-dimensional systems are stronger than for two qubits," Phys. Rev. Lett. **85**, 4418–4421 (2000).
13. V. Karimipour, A. Bahraminasab, and S. Bagherinezhad, "Quantum key distribution for *d*-level systems with generalized bell states," Phys. Rev. A **65**, 042320 (2002).

#132709 - $15.00 USD Received 2 Aug 2010; revised 9 Sep 2010; accepted 7 Oct 2010; published 10 Dec 2010

14. N. J. Cerf, M. Bourennane, A. Karlsson, and N. Gisin, "Security of quantum key distribution using d-level systems," Phys. Rev. Lett. **88**, 127902 (2002).
15. B. P. Lanyon, M. Barbieri, M. P. Almeida, T. Jennewein, T. C. Ralph, K. J. Resch, G. J. Pryde, J. L. O'Brien, A. Gilchrist, and A. G. White, "Simplifying quantum logic using higher-dimensional hilbert spaces," Nat. Phys. **5**, 134–140 (2009).
16. T. Vértesi, S. Pironio, and N. Brunner, "Closing the detection loophole in bell experiments using qudits," Phys. Rev. Lett. **104**, 060401 (2010).
17. This is strictly true for paraxial beams only.
18. E. Nagali, L. Sansoni, F. Sciarrino, F. D. Martini, L. Marrucci, B. Piccirillo, E. Karimi, and E. Santamato, "Optimal quantum cloning of orbital angular momentum photon qubits through hong-ou-mandel coalescence," Nat. Photon. **3**, 720–723 (2009).
19. E. Nagali, F. Sciarrino, F. D. Martini, L. Marrucci, B. Piccirillo, E. Karimi, and E. Santamato, "Quantum information transfer from spin to orbital angular momentum of photons," Phys. Rev. Lett. **103**, 013601 (2009).
20. E. Nagali, F. Sciarrino, F. D. Martini, B. Piccirillo, E. Karimi, L. Marrucci, and E. Santamato, "Polarization control of single photon quantum orbital angular momentum states," Opt. Express **17**, 18745–18759 (2009).
21. E. Nagali, L. Sansoni, L. Marrucci, E. Santamato, and F. Sciarrino, "Experimental generation and characterization of single-photon hybrid ququarts based on polarization and orbital angular momentum encoding," Phys. Rev. A **81**, 052317 (2010).
22. E. Nagali, D. Giovannini, L. Marrucci, S. Slussarenko, E. Santamato, and F. Sciarrino, "Experimental optimal cloning of four-dimensional quantum states of photons," Phys. Rev. Lett. **105**, 073602 (2010).
23. V. Y. Bazhenov, M. V. Vasnetsov, and M. S. Soskin, "Laser beams with screw dislocations in their wavefronts," Sov. Phys.–JETP Lett. **52**, 429–431 (1990).
24. J. Leach, M. J. Padgett, S. M. Barnett, S. Franke-Arnold, and J. Courtial, "Measuring the orbital angular momentum of a single photon," Phys. Rev. Lett. **88**, 257901 (2002).
25. J. Leach, J. Courtial, K. Skeldon, S. M. Barnett, S. Franke-Arnold, and M. J. Padgett, "Interferometric methods to measure orbital and spin, or the total angular momentum of a single photon," Phys. Rev. Lett. **92**, 013601 (2004).
26. M. J. Padgett and L. Allen, "Orbital angular momentum exchange in cylindrical-lens mode converters," J. Opt. B: Quantum Semiclassical Opt. **4**, S17–S19 (2002).
27. L. Marrucci, C. Manzo, and D. Paparo, "Optical spin-to-orbital angular momentum conversion in inhomogeneous anisotropic media," Phys. Rev. Lett. **96**, 163905 (2006).
28. L. Marrucci, C. Manzo, and D. Paparo, "Pancharatnam-Berry phase optical elements for wavefront shaping in the visible domain: switchable helical modes generation," Appl. Phys. Lett. **88**, 221102 (2006).
29. Suitable waveplates can be introduced to compensate the polarization change introduced by real Dove prism, but this is often unnecessary because the polarization change is very small [1–3].
30. E. Karimi, S. Slussarenko, B. Piccirillo, L. Marrucci, and E. Santamato, "Polarization-controlled evolution of light transverse modes and associated pancharatnam geometric phase in orbital angular momentum," Phys. Rev. A **81**, 053813 (2010).
31. Examples are the diagonal, antidiagonal, left-circular, right-circular polarizations.
32. M. Frede, R. Wilhelm, M. Brendel, C. Fallnich, F. Seifert, B. Willke, and K. Danzmann, "High power fundamental mode nd:yag laser with efficient birefringence compensation," Opt. Express **12**, 3581–3589 (2004).
33. E. A. Khazanov, O. V. Kulagin, S. Yoshida, D. B. Tanner, and D. H. Reitze, "Investigation of self-induced depolarization of laser radiation in terbium gallium garnet," IEEE J. Quantum Electron. **35**, 1116–1122 (1999).
34. N. F. Andreev, O. V. Palashov, A. K. Potemkin, D. H. Reitze, A. M. Sergeev, and E. A. Khazanov, "A 45-db faraday isolator for 100-w average radiation power," Quantum Electron. **30**, 1107–1108 (2000).
35. If the pure OAM eigenstates $|\ell\rangle$ are described by Laguerre-Gaussian modes, then the $|h_\ell\rangle$ and $|v_\ell\rangle$ states correspond to Hermite-Gaussian modes.
36. M. Fiorentino and F. N. Wong, "Deterministic controlled-not gate for single-photon two-qubit quantum logic," Phys. Rev. Lett. **93**, 070502 (2004).
37. L. Hardy, "Non locality for two particles without inequalities for almost all entangled states," Phys. Rev. Lett. **71**, 1665–1668 (1993).
38. E. Karimi, B. Piccirillo, L. Marrucci, and E. Santamato, "Light propagation in a birefringent plate with topological charge," Opt. Lett. **34**, 1225–1227 (2009).
39. N. González, G. Molina-Terriza, and J. P. Torres, "How a dove prism transforms the orbital angular momentum of a light beam," Opt. Express **14**, 9093–9102 (2006).
40. D. F. V. James, P. G. Kwiat, W. J. Munro, and A. G. White, "Measurement of qu-bit," Phys. Rev. A **64**, 052312 (2001).
41. M. J. Padgett and J. Courtial, "Poincaré-sphere equivalent for light beams containing orbital angular momentum," Opt. Lett. **24**, 430–432 (1999).

#132709 - $15.00 USD Received 2 Aug 2010; revised 9 Sep 2010; accepted 7 Oct 2010; published 10 Dec 2010

1. Introduction

It is well known that photons can carry two different types of angular momenta: the spin angular momentum (SAM), associated with the light polarization, and the orbital angular momentum (OAM), associated with the azimuthal distribution of the complex electrical field [4–7]. A circularly polarized beam carries $\sigma\hbar$ SAM per photon, where $\sigma = \pm 1$ corresponds to the handedness of polarization. A beam with azimuthal phase dependence of $\exp(i\ell\phi)$ (where ϕ is transverse azimuthal angular coordinate and ℓ is an integer) carries a definite OAM $\ell\hbar$ per photon [4]. SAM forms a two-dimensional Hilbert space and is one of the most used physical realizations of a qubit – fundamental unit in quantum information and cryptography [8]. The OAM space, instead, is inherently multidimensional and thus can be used for realization of qudits, i.e. multilevel (more than two) quantum states [9, 10]. Qudits are useful for increasing of the total amount of information carried by single photon [10,11], or to implement more complex quantum computation algorithms and protocols not applicable in the binary polarization space (see, e.g., Refs. [12–16]). The SAM and OAM spaces of the same photon, being independent from each other [17], can be used together for creating single-photon entangled (or non-separable) quantum states, including qudits [18–22]. Sorting photons according to their different polarization states is very easily accomplished by polarizing beamsplitters and birefringent waveplates. Sorting photons according to their different OAM modes is a more complex problem, although a number of techniques have been conceived to this purpose [23–26]. A very common technique to detect single photon OAM is based on "fork-like" computer-generated holograms used in combination with suitable pinhole or single-mode optical-fiber mode filtering [23]. However, this technique is affected by the low overall transmission efficiencies of the hologram and of the optical fiber (or pinhole) filtering system. Rarely the overall efficiency of such systems can exceed 40%. Alternative setups involve a Mach-Zehnder interferometer with two Dove prisms [24,25] or two confocal cylindrical lenses acting as OAM mode converters [26]. These techniques have a theoretical efficiency of 100% and may be used in the single photon regime, but require high mechanical stability, careful path matching of the arms of the interferometer and careful positioning and alignment of the cylindrical lenses, which makes them not very practical.

In this paper, we propose a novel OAM sorting interferometric setup based on a polarizing Sagnac interferometer (PSI) and a single Dove prism (DP). This setup, labeled PSI-DP in the following, ideally has a 100% efficiency, works with single photons, and has a good stability because of the self-compensation of the optical paths inside the interferometer. Moreover, the use of a single Dove prism further simplifies the setup. In the following, we will discuss and demonstrate experimentally the ability of the PSI-DP to sort photons carrying different OAM values, and will present some additional demonstrative applications of the PSI-DP in spin-orbit processing, such as the realization of a C-NOT gate, efficient photon spin-orbit Bell's states measurement and entanglement control of the spin-orbit Schmidt's state – a two-component non-maximally entangled state in the spin-orbit Hilbert space. These experiments required photons in definite OAM eigenstates that were generated and analyzed by means of auxiliary setups based on the q-plate (QP), a newly introduced device able to convert the photon spin into OAM by the spin-to-orbital conversion (STOC) process [27,28]. A brief overview of the QP and its action on the photon OAM is given in the experimental section below.

2. The Polarizing Sagnac Interferometer

Interferometer-based OAM sorting methods usually exploit the $\exp(i\ell\phi)$ spiraling phase form of the light beams carrying a definite value of OAM. When such beams are rotated around their axis through an angle α, the wavefront phase dependence changes into $\exp(i\ell(\phi+\alpha))$, so that a phase shift $\Delta\psi = \ell\alpha$ appears in the rotated beam. A device, that may be used to in-

#132709 - $15.00 USD Received 2 Aug 2010; revised 9 Sep 2010; accepted 7 Oct 2010; published 10 Dec 2010

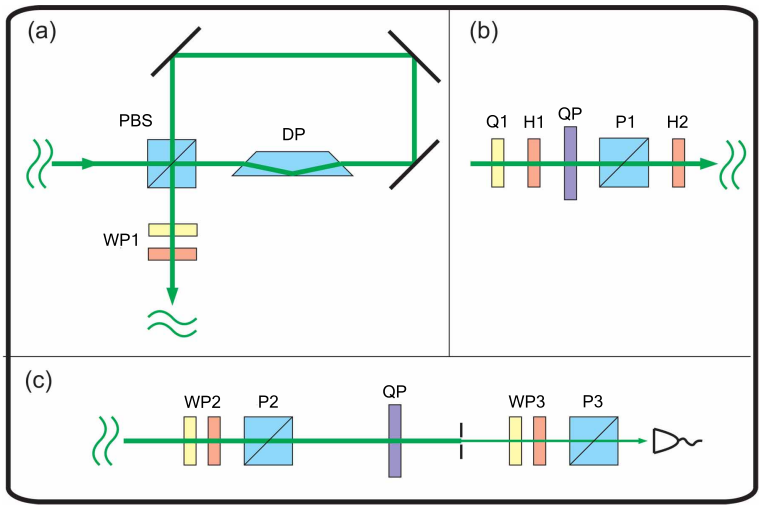

Fig. 1. (a) the polarizing Sagnac interferometer (PSI) with Dove prism (DP), or PSI-DP. (b) The auxiliary setup used to generate photons with OAM $\ell = \pm 2$. Some of the optical components were eventually placed or removed to create the input states for each experimental demonstration. (c) The auxiliary setup used to analyze photons with OAM $\ell = \pm 2$. The auxiliary setups in (b) and (c) use a q-plate (QP) to convert the photon spin into OAM and viceversa. Legenda of other symbols: PBS - polarizing beam-splitter; WP - generic waveplate; Q - quarter-wave plate; H - half-wave plate; P - polarizer.

duce such beam rotation is the DP. The DP flips the transverse cross section of the transmitted beam, so that two DPs, rotated at angle α with respect to each other induce an overall rotation of the transverse optical field of an angle 2α along the beam axis. DPs are commonly used in periscopes to maintain the image right when the periscope is rotated. As suggested by Leach [24] two DPs inserted in the arms of a Mach-Zehnder interferometer can be used to sort the incident photons according to their OAM. Here we used a single DP, instead, inserted in a PSI as shown in Fig. 1(a).

A single polarizing beam splitter (PBS) is used as entry and exit gate of the device. The PBS splits the incident beam into its horizontal ($|H\rangle$) and vertical ($|V\rangle$) components which circulate inside the interferometer along the same path, but in the opposite directions. After being reflected by the mirrors they recombine again and exit the interferometer from the other side of the PBS. Inserting in the PSI a single DP rotated through an angle α with respect to the interferometer plane is equivalent to inserting two DPs in the two arms of the Leach interferometer, rotated with respect of each other through an angle 2α. After passing through the interferometer, the two counter-propagating orthogonal polarizations $|H\rangle$ and $|V\rangle$ will gain a relative phase of $4\ell\alpha$. In this way, our setup is able to induce an ℓ-dependent change of the polarization state of the incident beam. The OAM sign remains unchanged, however, because the total number of reflections from mirrors, PBS, and DP is even for both polarizations. Neglecting scattering and absorption losses and assuming an ideal polarization preserving Dove prism [29], the theoretical transparency of the PSI-DP device is 100%. As shown in the next section, the PSI-DP can simulate the Leach interferometer for OAM photon sorting. But it should be noticed that the PSI-DP handles polarization too, so it can perform a wider set of operations in the OAM and also in the full photon spin-orbit space. For example, when qubits formed by opposite OAM eigenstates $|\pm\ell\rangle$ are considered, the PSI-DP may simulate a $\pi/2$ cylindrical lens converter, changing LG_ℓ modes into HG_ℓ modes [30]. The capability of doing complex operations in the

#132709 - $15.00 USD Received 2 Aug 2010; revised 9 Sep 2010; accepted 7 Oct 2010; published 10 Dec 2010

photon spin-orbit space, the need of a single Dove prism, and the robustness with respect mechanical solicitations due to the optical path self-compensation render the PSI-DP much more attractive than conventional Mach Zehnder- based interferometers in all applications were the photon OAM plays an important role. In the remaining part of this work, we will discuss some possible practical applications of the PSI-DP device, in order to demonstrate its potential.

2.1. The OAM sorter

The ℓ-dependent relative phase shift induced by the PSI-DP can be exploited for sorting input photons sharing the same polarization state according to their different OAM values into orthogonal polarization states of the exit beam. The further separation over different paths is then easily and efficiently accomplished by suitable waveplates and PBS. Let us assume the impinging photon having a definite value ℓ of OAM and definite polarization state $|\psi\rangle = a|H\rangle + b|V\rangle$. The input photon state is denoted by $|\psi,\ell\rangle$, where the first slot in the ket denotes the polarization state and the second slot the OAM state. The action of the PSI-DP with DP at angle α on such a photon state is given by

$$|\psi,\ell\rangle \xrightarrow{\widehat{PSI_\alpha}} ae^{2i\ell\alpha}|H,\ell\rangle + be^{-2i\ell\alpha}|V,\ell\rangle = -i\cos 2\ell\alpha|\psi,\ell\rangle + \sin 2\ell\alpha|\psi',\ell\rangle) \tag{1}$$

where $|\psi'\rangle = a|H\rangle - b|V\rangle$. We see that for input states with equally weighted H and V polarizations (i.e. states with $|a|^2 = |b|^2 = 1/2$), the states $|\psi'\rangle$ and $|\psi\rangle$ are orthogonal, so that they can be easily separated. In this work we assume always equally weighted input polarization states [31]. Then, from Eq. (1) we see that if $2\ell\alpha = k\pi$ (integer k) the polarization state remains unchanged (up to a global phase factor), while if $2\ell\alpha = \pi/2 + k\pi$ the polarization state becomes orthogonal to the incident one. Setting, for example, the angle of the DP to $\alpha = \pi/4$ the PSI-DP changes the polarization of the photons that carry odd values of OAM to the orthogonal state $|\psi'\rangle$, while the photons that carry even values of OAM remain in their $|\psi\rangle$ polarization state. Using a half-wave plate (HWP), with optical axis rotated through an angle of $\pi/8$, and a PBS placed after the PSI-DP, the even and odd values of OAM are spatially separated for detection purposes. One or more cascaded PSI-DPs may work as an OAM eigenstates sorter in the same way as the Leach interferometer [24,25]. As the Leach interferometer, the PSI-DP works in the single-photon regime and has nominal 100% transmission efficiency. The main advantages of the PSI-DP are the use of a single DP and the self-compensation of the optical paths so that no adjustments are required to obtain destructive interference. Unlike the Leach interferometer, however, the PSI-DP handles the OAM content of the two orthogonal polarizations in a different way. This peculiar feature can be exploited for applications different from the OAM photon sorting. A few examples are outlined below.

2.1.1. OAM qubit measurement

In many quantum optics experiments dealing with photon SAM and OAM, the OAM space is restricted to only two OAM eigenstates given in advance. This is due to the fact that two given eigenstates of a quantum system provide a qubit – the minimal unit of quantum information. Unlike in the photon spin case, however, where the two states have opposite eigenvalues, in the case of photon OAM we may form qubits with any pair of eigenvalues ℓ_1 and ℓ_2. Qubits must be created and than analyzed and detected. In the detection stage, different qubits must be sorted and sent onto different channels. In the case of the photon SAM this task is accomplished by a PBS. In the case of photon OAM qubits, this task is usually performed by suitable computer generated holograms (see [6,7] and references therein), whose efficiency rarely exceeds 40%. The OAM photon sorting can be accomplished with greater efficiency by the PSI-DP exploiting the ℓ-dependent relative phase shift to address photons with any prescribed pair of OAM values

#132709 - $15.00 USD Received 2 Aug 2010; revised 9 Sep 2010; accepted 7 Oct 2010; published 10 Dec 2010

ℓ_1 and ℓ_2 into orthogonal polarization states of the exit beam. In fact, evaluating Eq. (1) for $\ell = \ell_1$ and $\ell = \ell_2$ and imposing that the output polarization states are orthogonal, we find the condition

$$\cos 2(\ell_2 - \ell_1)\alpha = 0 \;\Rightarrow\; \alpha = \frac{(2k+1)\pi}{4(\ell_2 - \ell_1)} \tag{2}$$

with integer k. In most quantum optics experiments, OAM states with opposite values of ℓ are prescribed. To discriminate the states $|+\ell\rangle$ and $|-\ell\rangle$, the DP must be set at $\alpha = \pi/8\ell$. The two orthogonal polarizations at the PSI-DP output are then sent into different paths by conventional PBS. When configured in this way, the PSI-DP behaves as an OAM beam-splitter. The contrast ratio and overall transmission are limited only by constructive defects, so they may be very large as shown in the experimental section.

2.1.2. OAM subspace purification

As said above, in many quantum applications qubits are formed combining the $|+\ell\rangle$ and $|-\ell\rangle$ OAM eigenstates, as they are not affected by Gouy dephasing effects [19]. In these cases, it may be of some importance to clean up the beam from all other OAM components. Because the OAM eigenstates are usually originated from TEM_{00} laser beams, it is of particular interest to clean up the beam from any residual $\ell = 0$ OAM component. The PSI-DP can be used to this purpose by simply setting the angle of the DP at $\alpha = \pi/(4\ell)$ and polarizing the input photon along the antidiagonal direction. In fact, when Eq. (1) with $\alpha = \pi/(4\ell)$ is applied to the qutrit $|\psi_{in}\rangle = a|A,0\rangle + b|A,-\ell\rangle + c|A,\ell\rangle$ we obtain the output state $|\psi_{out}\rangle$ as

$$|\psi_{out}\rangle = -ia|A,0\rangle + b|D,-\ell\rangle - c|D,\ell\rangle, \tag{3}$$

so that the input $\ell = 0$ component is left in its initial antidiagonal polarization state and the two $\pm\ell$ components are put into the orthogonal diagonal polarization state. The $\ell = 0$ component can be then easily separated from the ℓ and $-\ell$ by a PBS placed at the output port of the device. Such $\ell = 0$ filtering is very useful since most holograms, spiral phase plates, q-plates etc., commonly used to generate OAM eigenvalues from TEM_{00} beam, do not produce OAM eigenstates with 100% purity due to misalignment and inaccuracies of fabrication. It is worth noting that the $\ell = 0$ component of the input beam is not lost, but sent into one output port of the final PBS. We may then use the same device to filter out the nonzero OAM components leaving a very pure output TEM_{00} mode with no losses. This can be useful, for example, to face the serious problem of combining high power ($\simeq$ 100 W or more) with excellent beam quality, as e.g. in lasers systems [32] and Faraday isolators [33,34] currently developed for gravitational wave detection.

2.2. Spin-orbit quantum computation

Entangled non-separable photon spin-orbit states are at the core of many quantum information applications. Such states do not show the most notable property of entangled photon pairs – non-locality – nevertheless they exhibit paradoxical quantum features related to the quantum contextuality which render these single-photon entangled states very interesting for quantum computation purposes. In fact, operations like universal unitary gates, deterministic complete Bell measurement, etc., which are impossible in the two-photon case, can be realized in the case of single photons with entangled degrees of freedom. Our PSI-DP acts on the photon SAM and OAM simultaneously, so that it can realize some of the most important gates in the photon spin-orbit space, such as the C-NOT gate, the unitary gate for Bell's states measurement or a gate to generate spin-orbit states with controllable entanglement.

#132709 - $15.00 USD Received 2 Aug 2010; revised 9 Sep 2010; accepted 7 Oct 2010; published 10 Dec 2010

2.2.1. C-NOT gate

The controlled-NOT (C-NOT) gate is the key gate for most of the quantum algorithms based on two qubits. In fact, using C-NOT gates and global phase retarders it is possible to realize any unitary gate in the 4D two-qubit Hilbert space. The C-NOT gate flips the state of one of the qubits depending on the state of the other. If the logical basis of the two-qubit state is given by the four kets $|0,0\rangle$, $|0,1\rangle$, $|1,0\rangle$ and $|1,1\rangle$ and the first qubit is the control one, then the C-NOT gate action performs the following logical operation

$$|0,0\rangle \overset{\widehat{CNOT}}{\longrightarrow} |0,0\rangle; \quad |0,1\rangle \overset{\widehat{CNOT}}{\longrightarrow} |0,1\rangle; \quad |1,0\rangle \overset{\widehat{CNOT}}{\longrightarrow} |1,1\rangle; \quad |1,1\rangle \overset{\widehat{CNOT}}{\longrightarrow} |1,0\rangle. \tag{4}$$

If the spin-orbit space logical basis is given by $|R,-\ell\rangle$, $|R,\ell\rangle$, $|L,-\ell\rangle$ and $|L,\ell\rangle$, where L and R denote the left and right circular polarizations, the PSI-DP with the DP angle set to $\pi/8\ell$ performs an OAM C-NOT operation, changing the polarization state of the photons with OAM $+\ell$ into the orthogonal one and leaving the polarization of the photons with $-\ell$ unchanged. The exit polarization is transformed as $|R\rangle \longrightarrow |A\rangle$, $|L\rangle \longrightarrow |D\rangle$ for the negative OAM value and $|R\rangle \longrightarrow |D\rangle$, $|L\rangle \longrightarrow |A\rangle$ for the positive OAM value. To come back into the circular basis an additional quarter-wave plate with its optical axis oriented at 90° is needed beyond the PSI-DP so that the overall operation is given by

$$\begin{aligned} |L,\ell\rangle &\overset{\widehat{CNOT+QWP}}{\longrightarrow} |L,\ell\rangle; \quad |L,-\ell\rangle \overset{\widehat{CNOT+QWP}}{\longrightarrow} |R,-\ell\rangle; \\ |R,\ell\rangle &\overset{\widehat{CNOT+QWP}}{\longrightarrow} |R,\ell\rangle; \quad |R,-\ell\rangle \overset{\widehat{CNOT+QWP}}{\longrightarrow} |L,-\ell\rangle \end{aligned} \tag{5}$$

The PSI-DP behaves as a C-NOT gate with the polarization as control qubit, if we take as logical basis the states $|H,h_\ell\rangle$, $|H,v_\ell\rangle$, $|V,h_\ell\rangle$ and $|V,v_\ell\rangle$, where $|h_\ell\rangle = (|\ell\rangle + |-\ell\rangle)/\sqrt{2}$ and $|v_\ell\rangle = (|\ell\rangle - |-\ell\rangle)/i\sqrt{2}$ are the superpositions of OAM states, equivalent to the horizontal and vertical polarization states [35]. In this case the OAM state of the $|H\rangle$ and $|V\rangle$ component will be rotated through an angle of $\pm\pi/4\ell$ respectively and the state of the outgoing photon is given by

$$\begin{aligned} |V,v_\ell\rangle &\overset{\widehat{CNOT}}{\longrightarrow} |V,d_\ell\rangle \overset{\widehat{DP}}{\longrightarrow} |V,v_\ell\rangle; \quad |V,h_\ell\rangle \overset{\widehat{CNOT}}{\longrightarrow} |V,a_\ell\rangle \overset{\widehat{DP}}{\longrightarrow} |V,h_\ell\rangle \\ |H,v_\ell\rangle &\overset{\widehat{CNOT}}{\longrightarrow} |H,a_\ell\rangle \overset{\widehat{DP}}{\longrightarrow} |H,h_\ell\rangle \quad |H,h_\ell\rangle \overset{\widehat{CNOT}}{\longrightarrow} |H,d_\ell\rangle \overset{\widehat{DP}}{\longrightarrow} |H,v_\ell\rangle, \end{aligned} \tag{6}$$

where $|a_\ell\rangle$ and $|d_\ell\rangle$ are the OAM states equivalent to the antidiagonal and diagonal polarization states. The final transformation $|d_\ell\rangle \rightarrow |v_\ell\rangle$ and $|a_\ell\rangle \rightarrow |h_\ell\rangle$ to return back into the initial basis is done by a second DP rotated at angle $\pi/8\ell$, placed beyond the PSI-DP. The use of the PSI-DP as a polarization C-NOT gate in the photon polarization-path space was already reported [36].

2.2.2. Bell's states measurements

A well known theorem forbids deterministic and 100% efficient detection of all the four Bell's states of a photon pair with a process that involves just linear optics. Up to now, the experimental realization of the Bell's states detection involves additional degrees of freedom, higher order entanglement, or give probabilistic result with non-unit fidelity. The situation is different in the case of single-particle entanglement, where such measurement is possible. The PSI-DP with a DP oriented at angle $\pi/8\ell$ realizes an unitary optical gate which transforms each one of the four Bell states

$$\begin{aligned} |B_1\rangle &= (|H,h_\ell\rangle + |V,v_\ell\rangle)/\sqrt{2}; \qquad |B_2\rangle = (|H,h_\ell\rangle - |V,v_\ell\rangle)/\sqrt{2}; \\ |B_3\rangle &= (|H,v_\ell\rangle + |V,h_\ell\rangle)/\sqrt{2}; \qquad |B_4\rangle = (|H,v_\ell\rangle - |V,h_\ell\rangle)/\sqrt{2} \end{aligned}$$

#132709 - $15.00 USD Received 2 Aug 2010; revised 9 Sep 2010; accepted 7 Oct 2010; published 10 Dec 2010

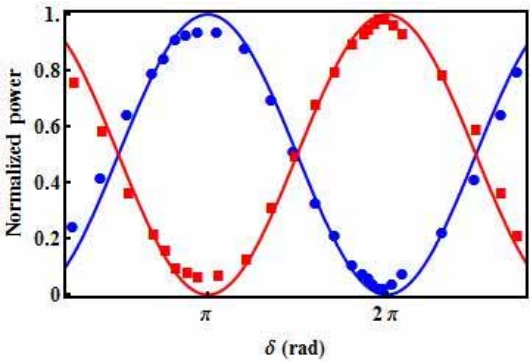

Fig. 2. Filtering the TEM_{00} mode from the OAM carrying beam. Squares ($\ell = 2$) and dots ($\ell = 0$) represent the normalized intensities of the two exits of the final PBS $P2$ in Fig. 1(c), as functions of the QP optical retardation δ. The solid curves are best fits with $\sin^2 \delta/2$ and $\cos^2 \delta/2$ behavior expected from Eq. (8). The experiment was repeated for $\ell = -2$ with similar results.

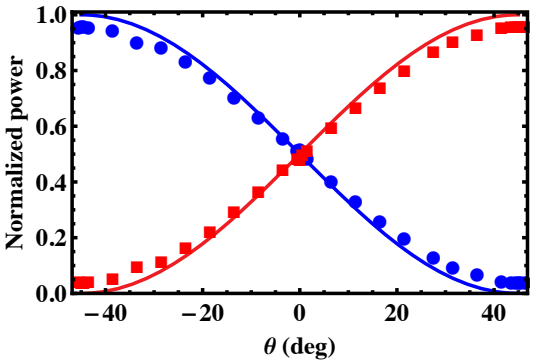

Fig. 3. Sorting of the OAM eigenstates $|\pm 2\rangle$. Dots ($\ell = 2$) and squares ($\ell = -2$) represent normalized intensities of the two exits of the final PBS in Fig. 1(c), as functions of the angle θ of the half-wave plate (HWP), that controls the state of the input beam. The solid line is given by $\sin^2(\theta - \pi/4)$ and $\cos^2(\theta - \pi/4)$, according to theory.

into the not entangled spin-orbit basis $|H, h_\ell\rangle$, $|V, v_\ell\rangle$, $|V, h_\ell\rangle$ and $|H, v_\ell\rangle$. The last states can be analyzed with standard techniques to measure the photon SAM and the OAM separately. The Bell state analysis gate can be realized by mounting the PSI-DP as a polarization C-NOT gate, as described in the previous section, to obtain $|B_1\rangle \to |A, v\rangle$, $|B_2\rangle \to |D, v\rangle$, $|B_3\rangle \to |A, h\rangle$, $|B_4\rangle \to |D, h\rangle$. Finally, a HWP at 22.5° can be used to rotate the photon polarization back into the horizontal plane.

2.2.3. Schmidt state generation

It is well known that any two-qubit state, such as the photon spin-orbit state, can be put into the general Schmidt form

$$|\Psi_S\rangle = \cos(\theta)|H, h_\ell\rangle - \sin(\theta)|V, v_\ell\rangle \tag{7}$$

by means of unitary transformations acting on each degree of freedom separately. Conversely, given the state [Eq. (7)], any spin-orbit state can be obtained by applying separate unitary transformations to the SAM and OAM degrees of freedom. The degree of entanglement of the

#132709 - $15.00 USD Received 2 Aug 2010; revised 9 Sep 2010; accepted 7 Oct 2010; published 10 Dec 2010

state [Eq. (7)] is parametrized by the angle θ. The non-maximally entangled state [Eq. (7)] could be used, for example, to demonstrate the Hardy paradox [37] – a test of the quantum nature of the entanglement and a proof of contextuality (or in the case of two-particles – non-locality) of quantum mechanics.

3. Experiment

Since quantum optics experiments that involve single-photon entanglement can be simulated using coherent CW laser source, to test experimentally our PSI-DP scheme we used a c.w. vertically polarized 532 nm TEM_{00} single frequency laser beam. To generate beams carrying nonzero OAM, we used the auxiliary setup shown in Fig. 1(b) based on the use of a q-plate (QP) [27,28]. The QP was placed after a set of quarter-wave plate $Q1$, half-wave plates $H1, H2$ and polarizer $P1$. Some of the optical components were removed or inserted back, depending on the desired photon state. Our QP had an unit topological charge and produced OAM eigenvalues of order $|\ell| = 2$. The action on the QP on the circular polarizations is given by [27]

$$\begin{aligned} |L,\ell\rangle &\xrightarrow{\widehat{QP}} \cos(\delta/2)|L,\ell\rangle - i\sin(\delta/2)|R,\ell+2\rangle, \\ |R,\ell\rangle &\xrightarrow{\widehat{QP}} \cos(\delta/2)|R,\ell\rangle - i\sin(\delta/2)|L,\ell-2\rangle \end{aligned} \tag{8}$$

where δ is the q-plate optical retardation. When the QP is tuned to a half-wave retardation ($\delta = \pi$) pure $\ell = \pm 2$ OAM eigenmodes are generated from a circularly polarized TEM_{00} input beam. In our experiments to test the PSI-DP the optical retardation δ of the q-plate was adjusted by thermal tuning [38]. Once tuned, the q-plate can generate any qubit in the $\ell = \pm 2$ OAM Hilbert subspace starting from an elliptically polarized TEM_{00}, according to [19]

$$\alpha|L,0\rangle + \beta|R,0\rangle \longrightarrow \frac{1}{\sqrt{2}}|H\rangle(\alpha|2\rangle + \beta|-2\rangle) \tag{9}$$

where a polarizer after the q-plate was used to select the H polarization. The insertion of the polarizer reduces the conversion efficiency upper limit to 50% of the incident photons [19,20]. The spin-to-OAM conversion process (STOC) in Eq. (9) is reversible and allows one to transfer back any OAM qubit into a corresponding polarization qubit according to

$$\alpha|H,2\rangle + \beta|H,-2\rangle \longrightarrow \frac{1}{\sqrt{2}}(\alpha|L,0\rangle + \beta|R,0\rangle). \tag{10}$$

The inverse STOC process is very useful in the detection stage, because the information encoded in the OAM degree of freedom is transferred into the light polarization, which is very easy to be analyzed. The auxiliary setup used for the OAM measurement is shown in Fig. 1(c). The photon state coming from the PSI-DP was first analyzed in polarization by the waveplates $WP2$ and PBS $P2$ and then the QP was used to transfer the OAM state into the corresponding polarization state of TEM_{00} mode [Eq. (10)], which was subsequently analyzed by waveplate $WP3$ and polarizer $P3$. The TEM_{00} mode in the output beam was selected by a spatial filter made by microscope objective and pinhole (not shown in the figure) [23]. The PSI-DP setup is shown in Fig. 1(a). At the PSI exit port the set of waveplates WP1 was inserted to compensate for the polarization changes due to the Dove prism, mirrors and PBS. The Dove prism, in particular, introduces a slight change in the light polarization [1–3,39] so that a fraction of light exits from the wrong port, increasing the PSI-DP losses. A straightforward calculations for our Dove prism (BK7 glass, 45° base angles) shows, however, that the losses due to the light depolarization by the Dove prism do not exceed 2% at our rotation angles. The observed average overall transmittance of the PSI-DP was about 80%, so it is mainly due to scattering

#132709 - $15.00 USD Received 2 Aug 2010; revised 9 Sep 2010; accepted 7 Oct 2010; published 10 Dec 2010

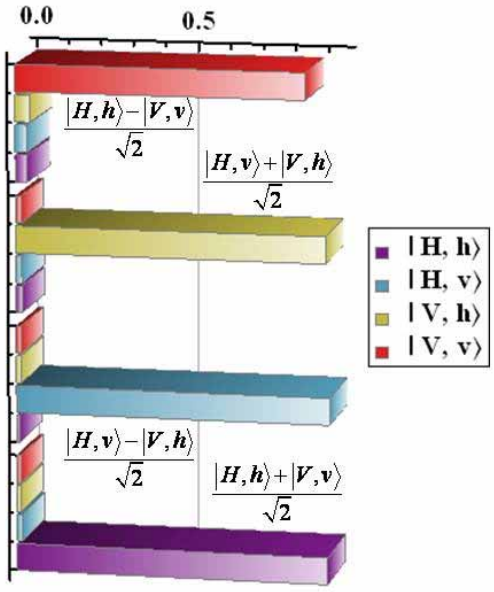

Fig. 4. Bell's state detection. The photons coming from the PSI-DP were first sorted by a PBS into their H and V polarizations and then sorted again by a QPs in each channel so to send the OAM h and v states into orthogonal polarizations and TEM_{00} mode by inverse STOC. The TEM_{00} mode was selected by a small aperture located beyond the QP.

and reflection losses from other optical components (we used no antireflection coating). We performed a few demonstrative experiments to test the different operations of the PSI-DP.

In the first experiment, we used the PSI-DP to clean up the TEM_{00} mode from the input beam (see Sec. 2.1.2). The input light was circularly polarized and sent into a QP. The optical retardation δ of the QP was changed so to obtain a mixture of $\ell = 0$ and $\ell = 2$ OAM eigenstates, according to Eq. (8). The polarizer $P1$ ensured antidiagonal polarization at the PSI input and the DP was rotated at $\alpha = \pi/8$. Figure 2 shows the data for the case $\ell = 2$. The $\ell = 2$ and $\ell = 0$ modes, shown in the figure, exit from the opposite ports of PBS $P2$ in Fig. 1(c). The measured contrast ratio of our cleaner was about 3.5:100.

In the second experiment, we used the PSI-DP to separate opposite OAM eigenstates. The input state was created by sending the H-polarized laser light into a HWP at angle $\theta/2$, a QWP at 45° and finally into a QP tuned for optimal STOC, so to obtain beyond the polarizer $P1$ of Fig. 1 the OAM qubit $|\Phi\rangle = \cos 2\theta|+2\rangle - \sin 2\theta|-2\rangle$ with antidiagonal polarization. After the QP tuning, the residual $\ell = 0$ component was negligible (less 1%). The OAM qubit superposition was changed by rotating the HWP. The DP in the PSI-DP was set at $\alpha = \pi/16$. The experimental results are shown in Fig. 3. The contrast ratio was 4.2:100 and the transmission efficiency larger than 90%, much larger than what can be obtained by holograms and spatial-filter combination.

In the third experiment, we implemented Bell's states detection with the PSI-DP. The states [Eq. (7)] can be generated with a QP with 100% efficiency. The states $|B_1\rangle$ and $|B_4\rangle$ are generated directly by sending in the QP a H and V-polarized TEM_{00} beam, respectively. The states $|B_3\rangle$ and $|B_2\rangle$ require an additional HWP at 45° beyond the QP, so to exchange the polarization states. The states [Eq. (7)] were disentangled by the PSI-DP C-NOT operation described in Sec. 2.2.1 with DP rotated at $\alpha = \pi/16$. The output base states $|H,h\rangle$, $|H,v\rangle$, $|V,h\rangle$ and $|V,v\rangle$

#132709 - $15.00 USD Received 2 Aug 2010; revised 9 Sep 2010; accepted 7 Oct 2010; published 10 Dec 2010

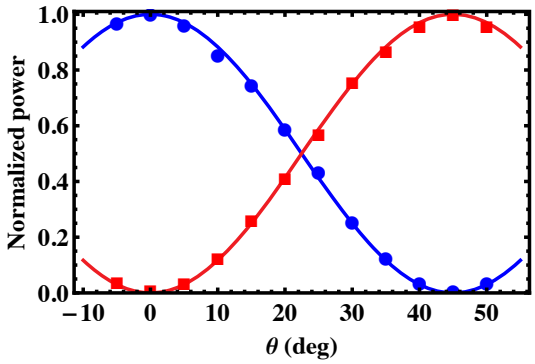

Fig. 5. Normalized intensities, corresponding to the $|H,h\rangle$ (dots) and $|V,v\rangle$ (squares) component of the state (7) as functions of the angle θ of the HWP. Solid lines correspond to $\cos^2(2\theta)$.

were analyzed in polarization and OAM separately by sending them into the four output channels of a setup formed by PBS and QPs with pinhole for inverse STOC. The average contrast ratio in separating the $|h\rangle$ and $|v\rangle$ OAM state by the inverse STOC was 1.4:100. The intensities of the signals at each one of the four exit gates of our analysis setup are shown in Fig. 4. At least 94% of the intensity was concentrated in one exit gate at once, showing very good disentanglement by the C-NOT PSI-DP operation.

In our final experiment, we used the PSI-DP to create the photon spin-orbit Schmidt state [Eq. (7)]. Although some photon spin-orbit states of the Schmidt form can be generated by simply sending through a QP an elliptically polarized TEM_{00} beam, this is not true for the state [Eq. (7)]. This is because some unitary operations, as $\pi/2$-conversion, for example, are difficult to be implemented in the OAM subspace and require cylindrical lens converters (the Dove prism performs a π-conversion). Our PSI-DP can do the OAM state $\pi/2$-conversion [30] and, hence, it can be exploited to create states as [Eq. (7)]. In our experiment, we first turned the laser beam polarization into diagonal and then sent it through the QP and PBS to obtain with 50% nominal efficiency the state $|H,d_\ell\rangle$, with $\ell = 2$, in our case. The state $|H,d_\ell\rangle$ was then made to pass through a HWP at angle θ and sent directly into the PSI-DP with Dove prism at $\alpha = \pi/8\ell = \pi/16$. A straightforward calculations shows that the photon spin-orbit state at the PSI exit is precisely the Schmidt state [Eq. (7)] with θ replaced by 2θ. The degree of entanglement of this spin-orbit state is controlled by rotating the HWP. We measured the intensity the $|H,h\rangle$ and $|V,v\rangle$ components of the Schmidt state generated by the PSI-DP with the same apparatus used for the SAM and OAM analysis in the previous experiment on Bell states. The results are reported in Fig. 5.

For the sake of completeness we measured by full spin-orbit tomography the density matrix of one of the states with maximal spin-orbit entanglement. The tomographic technique is commonly used in single photon quantum optics to measure qubits [40] and can be used also to characterize OAM photon states or even spin-orbit photon states [21,30,41]. The main advantage of tomography is that both the amplitude and phase of the optical field can be retrieved without having recourse to interferometers.The basic idea is to measure the Stokes parameters $s_i (i = 1,\ldots,3)$ by intensity differences in the left/right circular basis, in the horizontal/vertical basis and in the antidiagonal/digonal basis for the polarization qubit and in similar bases for the OAM qubit [40]. In our measurements the tomography was carried out by using PBS and QPs with pinhole for inverse STOC as in the previous experiments. The results are shown in Fig. 6 and are in excellent agreement with theory. The measured average fidelity defined as

#132709 - $15.00 USD Received 2 Aug 2010; revised 9 Sep 2010; accepted 7 Oct 2010; published 10 Dec 2010

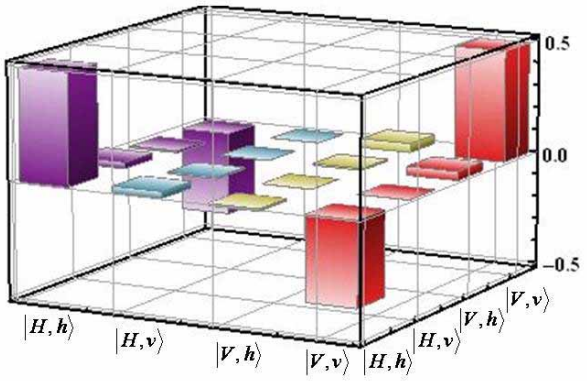

Fig. 6. Density matrix of the maximally entangled Hardy state, reconstructed by full spin-orbit tomography

the squared scalar product of the observed spin-orbit state and the expected state [Eq. (7)] was 92%.

4. Conclusions

In conclusions, we introduced a new interferometric layout, a Polarizing Sagnac interferometer with a Dove prism, that can realize OAM state sorting and different spin-orbit quantum gates at the single photon level. The PSI-DP is more stable than Mach-Zehnder-based interferometers for OAM because of the self-compensated optical paths and it is easier to use because it requires only one Dove prism. Moreover the PSI-DP can do nontrivial operation in the spin-orbit space, as experimentally demonstrated by few examples. Useful applications of the PSI-DP as an OAM sorting device and as a realization of quantum unitary gates, such as OAM C-NOT gate, full Bell's states detection gate, and a gate to generate Schmidt's photon states with controllable spin-orbit entanglement have been realized in this work, but we are confident that many other will be surely envisaged in the near future.

Acknowledgments

We thank Ebrahim Karimi for help in the quantum tomography analysis and useful discussions. The project PHORBITECH acknowledges the financial support of the Future and Emerging Technologies (FET) programme within the Seventh Framework Programme for Research of the European Commission, under FET-Open grant number: 255914.

#132709 - $15.00 USD Received 2 Aug 2010; revised 9 Sep 2010; accepted 7 Oct 2010; published 10 Dec 2010

Deterministic qubit transfer between orbital and spin angular momentum of single photons

Vincenzo D'Ambrosio[1], Eleonora Nagali[1], Carlos H. Monken[2], Sergei Slussarenko[3], Lorenzo Marrucci[3], Fabio Sciarrino[1,4,*]

[1]*Dipartimento di Fisica, Sapienza Università di Roma, Roma 00185, Italy*
[2]*Departamento de Fisica, Universidade Federal de Minas Gerais, Caixa Postal 702, Belo Horizonte, MG 30161-970, Brazil*
[3] *Dipartimento di Scienze Fisiche, Università di Napoli "Federico II", Compl. Univ. di Monte S. Angelo, 80126 Napoli, Italy*
[4] *Istituto Nazionale di Ottica Applicata, Firenze, Italy*
[*]*Corresponding author: fabio.sciarrino@uniroma1.it*

Compiled September 29, 2011

In this work we experimentally implement a deterministic transfer of a generic qubit initially encoded in the orbital angular momentum of a single photon to its polarization. Such transfer of quantum information, completely reversible, has been implemented adopting a electrically tunable q-plate device and a Sagnac interferomenter with a Dove's prism. The adopted scheme exhibits a high fidelity and low losses.

OCIS codes: (270.0270) Quantum Optics, (270.5585) Quantum information and processing

Qubits are often encoded in the polarization state of photons. This is essentially due to the ease of manipulation and detection of the spin angular momentum (SAM) of light. Besides SAM, photons can carry orbital angular momentum (OAM) [1], which is related to the spatial distribution of the field. Photon states with a well defined orbital angular momentum are the ones characterized by an azimuthal dependence $e^{il\phi}$ of the phase front, where l is an integer (e.g. Laguerre-Gauss modes) [2]. The Hilbert space associated with the OAM degree of freedom is infinite-dimensional, while the one associated with polarization is restricted to two dimensions. This fact suggests the use of OAM, alone or coupled with spin, as a resource to encode information in higher dimensional quantum states, or qudits [3–5]. A number of devices have been developed for the generation and manipulation of OAM photon eigenstates, including holograms [2, 6], mode converters [7], spiral phase plates [8], and more recently the liquid-crystal q-plate (QP) [9]. The latter device, in particular, introduces a controlled coupling between spin and orbital angular momentum of a single photon, allowing for a coherent transfer of information between the spaces associated with these two degrees of freedom [10]. This feature has been recently exploited for implementing a probabilistic quantum transferrer, i.e. a device that can transfer a qubit from a degree of freedom to another and *vice versa* with a theoretical success probability of 50% [11]. The transfer has been demonstrated in particular from the bidimensional space of polarization π to a bidimensional subspace of OAM $o_{|l|}$. A second qubit can then be added in the π space, once that the $\pi \rightarrow o_{|l|}$ transfer has been completed [4, 10]. The probabilistic nature of the demonstrated implementation is due to elements in the setup that discard half of the information encoded in different OAM subspaces ($o_{|l|} \rightarrow \pi$) or in the polarization ($\pi \rightarrow o_{|l|}$). However, a useful quantum information processing requires high efficiencies. Therefore, the demonstration of a lossless transferrer, ideally allowing for a qubit transfer with certainty (success probability $p = 1$), is an important goal. Schemes have been proposed in order to achieve this goal [11], but hitherto they have not been demonstrated experimentally.

In this paper we report the experimental implementation of a deterministic transferrer $o_2 \rightarrow \pi$ based on a q-plate and a polarizing Sagnac interferometer. In particular in this experiment we employ q-plates with topological charge $q = 1$ with tuning controlled by an electric field, which allows to achieve a higher efficiency of the device, and motorized wave-plates, so that the transfer process is entirely automatized. Moreover, the same experimental setup can be also used for the inverse, $\pi \rightarrow o_2$ process, by reversing the propagation direction of light.

Let us first describe the working principle of the deterministic transferrer, considering the $o_{|l|} \rightarrow \pi$ process. Let us assume that the incoming photon is prepared in an arbitrary OAM and fixed polarization state, so that all information is encoded in the OAM:

$$|H\rangle_\pi |\phi\rangle_{o_{|l|}} = |H\rangle_\pi \left(\alpha|+l\rangle + \beta|-l\rangle\right)_{o_{|l|}} \quad (1)$$

where H/V denotes the horizontal/vertical linear polarization. The state passes through a half waveplate (HWP) rotated at $\pi/8$ which transforms the polarization in a diagonal one: $|A\rangle = \frac{|H\rangle+|V\rangle}{2}$, so that the state reads:

$$|H\rangle_\pi \left(\alpha|+l\rangle + \beta|-l\rangle\right)_{o_{|l|}} + |V\rangle_\pi \left(\alpha|+l\rangle + \beta|-l\rangle\right)_{o_{|l|}} \quad (2)$$

Hereafter the indices π and $o_{|l|}$ are omitted for brevity. The photon is then sent into a polarizing Sagnac interferometer (PSI) with a polarizing beam-splitter (PBS) input/output port and a Dove prism (DP) in one of its arms [11, 12]. Defining γ as the angle between the base of the prism and the plane of the interferometer, the action of the DP on the counter-propagating H/V linear polarization components with generic OAM l is described by the following equations:

$$|H\rangle|l\rangle \rightarrow e^{2il\gamma}|H\rangle|l\rangle, \quad (3)$$

$$|V\rangle|l\rangle \rightarrow e^{-2il\gamma}|V\rangle|l\rangle \quad (4)$$

where the OAM-inverting effect of the reflections can be ignored, for simplicity, as long as the total number of reflections in the setup is even. Thus the two components of state 2 in the PSI evolve as:

$$\alpha|H\rangle|+l\rangle+i\beta|H\rangle|-l\rangle \rightarrow \alpha e^{2i\gamma l}|H\rangle|+l\rangle+i\beta e^{-2i\gamma l}|H\rangle|-l\rangle,$$

$$\alpha|V\rangle|+l\rangle-i\beta|V\rangle|-l\rangle \rightarrow \alpha e^{-2i\gamma l}|V\rangle|+l\rangle-i\beta e^{2i\gamma l}|V\rangle|-l\rangle.$$

Setting $\gamma = \pi/(8l)$ and applying these transformations to state 2, one obtains (up to a global phase factor) the output state:

$$\alpha|R\rangle|+l\rangle+\beta|L\rangle|-l\rangle$$

where L/R denote left/right circular polarization. By passing through a q-plate, such state is hence transformed in:

$$(\alpha|L\rangle+\beta|R\rangle)|0\rangle_o = |\phi\rangle_\pi|0\rangle_o$$

that completes the transfer. Since all the intermediate transformation steps are unitary, they are deterministic and reversible. The inverse process $\pi \rightarrow o_{|l|}$, is therefore obtained by simply inverting the light propagation through the same components. It is also interesting to note that the action of the transferrer is not limited to a $+l$ and $-l$ OAM subspace, but it works with any pair l_1, l_2 of OAM values. By repeating the analysis above, one finds that the transfer is ensured as long as the following general condition on the DP angle is satisfied:

$$\gamma = \frac{\pi}{4(l_1 - l_2)} \tag{5}$$

In this more general case, however, the final polarization state is not R but depends on the values of OAM involved.

The experimental setup we used for demonstrating the deterministic $o_2 \rightarrow \pi$ transfer process can be divided in three sections: (i) generation of single photons carrying the OAM input qubit, (ii) quantum transferrer, and (iii) output state analysis (see Fig.1). In section (i) of the apparatus, an ultraviolet (UV) beam with wavelength $\lambda_p = 397.5$ nm pumps a 1.5 mm thick nonlinear crystal of β-barium borate (BBO), which generates, through the spontaneous parametric down-conversion (SPDC) process, pairs of photons in spatial modes k_A and k_B with the same wavelength $\lambda = 795$ nm and orthogonal linear polarizations H and V. The two photons in k_A and k_B are then spectrally purified by interference filters with bandwidth $\Delta\lambda = 3$ nm. The photon in mode k_A is detected and acts as a trigger of the single-photon generation. The photon in mode k_B is delivered to the main setup via a single mode fiber, thus defining its transverse spatial mode to a pure TEM_{00}, corresponding to OAM $l = 0$. After the fiber output, two wave plates compensate the polarization rotation introduced by the fiber and a polarizing beam-splitter (PBS) projects the photon onto the state $|H\rangle_\pi$. A quarter waveplate (QWP) and a half-waveplate (HWP) are then used for encoding an arbitrary qubit in the polarization degree of freedom of the photon, as in Eq. (1). Finally, this polarization-encoded qubit is converted into a OAM-encoded one using the $\pi \rightarrow o_2$ *probabilistic* transferrer, as described in [10, 11]. For this step we used a q-plate with $q = 1$ combined with a PBS, providing conversion into the photon state

$$|\phi\rangle_{o_2} = \alpha|+2\rangle+\beta|-2\rangle \tag{6}$$

with a probability $p = 0.5$. This completes the input state preparation stage of our apparatus (generation box in Fig.1).

This preparation stage was used in particular for generating all states belonging to the three mutually unbiased bases spanning the bidimensional OAM subspace with $l = \pm 2$ (o_2): $\{|+2\rangle, |-2\rangle\}, \{|h\rangle, |v\rangle\}, \{|a\rangle, |d\rangle\}$, where, analogously to the polarization case, we define linear superpositions of $|+2\rangle$ and $|-2\rangle$ as $|h\rangle = \frac{1}{\sqrt{2}}(|+2\rangle+|-2\rangle), |v\rangle = \frac{1}{i\sqrt{2}}(|+2\rangle-|-2\rangle)$ and $|a\rangle = \frac{1}{\sqrt{2}}(|h\rangle+|v\rangle), |d\rangle = \frac{1}{\sqrt{2}}(|h\rangle-|v\rangle)$.

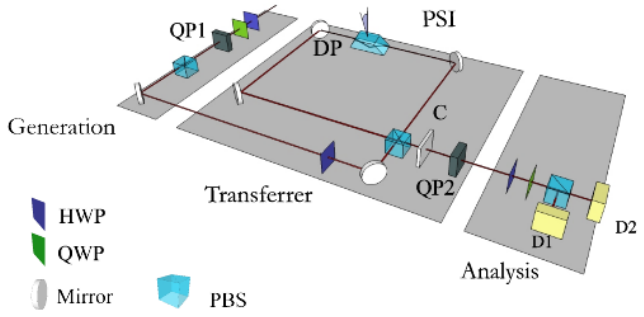

Fig. 1. Experimental setup adopted for the implementation of the deterministic quantum transferrer $o_2 \rightarrow \pi$. The input photon, coming from the left, is prepared by a probabilistic transferrer ($\pi \rightarrow o_2$) (first two waveplates, QP1 and PBS) into an arbitrary o_2 state with polarization H. After this generation stage, the PSI and the QP2 realize the deterministic transferrer ($o_2 \rightarrow \pi$). The outgoing polarization state is analyzed in the last part of the setup (waveplates, PBS, detectors D1 and D2). C is a phase compensation stage to correct all the unwanted phase shifts introduced by the setup. All q-plates are electrically tuned.

For the layout of the quantum transferrer setup, i.e. section (ii) of the apparatus, we refer to Fig. 1. The input qubit $|\phi\rangle_{o_2} = \alpha|+2\rangle+\beta|-2\rangle$ prepared in the previous section is now passed through a half wave plate in order to set the polarization to the diagonal state $|A\rangle$ and then injected in the PSI. The first PBS of the Sagnac interferometer splits the two polarizations in two opposite directions within the PSI, both passing through a DP rotated at angle $\gamma = \frac{\pi}{16}$. The state is then sent through a q-plate (QP2), which transforms the input state to $\alpha|L\rangle+\beta|R\rangle = |\varphi\rangle_\pi$ with $l = 0$ (mainly TEM_{00} mode). Thus the information initially encoded in the orbital angular momentum has been transferred to the polarization degree of freedom.

We note that both q-plates employed in this experiment are electrically tunable. In this device, the q-plate birefringence phase retardation δ is controlled by an external electric field which changes the orientation of the liquid crystal molecular director. This allows a more convenient control of the q-plate and a faster time response as compared to the thermally-tuned q-plate [13, 14]. By varying the applied voltage (with a sinusoidal signal) above the Fréedericksz threshold, the phase δ varies continuously between 0 and π (or more, depending on the cell thickness). This in turn leads to a varying con-

version efficiency of the q-plate, related to δ by a sinusoidal relation [11]. When $\delta = \pi$ the q-plate acts as a half wave plate on the polarization, which corresponds to the maximum value of conversion efficiency (tuned q-plate). In Fig.2-**a** we report as an example the characteristic curve of QP1, where it is shown that the optimal conversion efficiency is found to be around 4.5 V.

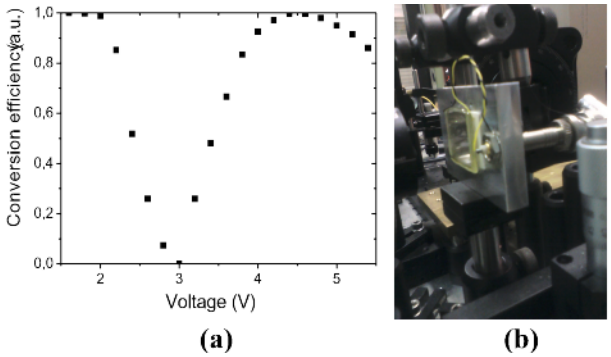

Fig. 2. **(a)** Conversion efficiency of the q-plate QP1 as a function of the applied voltage. Above the threshold voltage (around 2.2 V), the conversion efficiency of the q-plate can be adjusted, achieving its maximum around 4.5 V. **(b)** Photo of the q-plate.

After passing through the PSI and the second q-plate, all the information encoded in the input qubit is transferred to the polarization, and thus can be analyzed by a standard analysis setup made of waveplates and a polarizing beam splitter, which form the final section (iii) of our apparatus. The transmitted and reflected photons from the PBS are coupled to single mode fibers and detected by single photon counter modules D_1 and D_2. For full qubit tomography, the output of the deterministic transferrer has been analyzed in the three polarization bases $\{|R\rangle, |L\rangle\}, \{|H\rangle, |V\rangle\}, \{|A\rangle, |D\rangle\}$, recording the coincidence counts between detectors $[D_1, D_T]$ and $[D_2, D_T]$. The overlap between the input OAM qubit and the polarization output one after the transferrer has been estimated through the fidelity parameter $F = \frac{C_{max}}{C_{max}+C_{min}}$. All results are summarized in Table 1, showing that very good values of transfer fidelity are obtained.

Although ideally the implemented setup has success probability $p = 1$, the actual value is limited by standard optical losses in the optical components (mainly reflections, plus a little scattering and absorption) and by the final single-mode fiber coupling step that we used for experimental convenience and for mode purification, thus leading to an overall efficiency of 0.324. This value is three times larger than the one achieved with the probabilistic device [11]. The obtained improvement is attributed to the adoption of the deterministic scheme based on the Sagnac interferometer, to more efficient q-plates and to a better mode conversion exemplified by a higher single-mode coupling efficiency (compared to the one measured with previous q-plates) equal to 0.30. As further improvements the reflection losses could be reduced by adopting anti-reflection coating (in particular the q-plates are currently uncoated). Finally we note the single-mode fiber coupling (currently 0.5), although convenient for further processing of the output photons, is not a strictly required step.

State	Fidelity
$\|+2\rangle$	(0.994 ± 0.003)
$\|-2\rangle$	(0.992 ± 0.003)
$\|h\rangle$	(0.982 ± 0.005)
$\|v\rangle$	(0.944 ± 0.008)
$\|a\rangle$	(0.992 ± 0.003)
$\|d\rangle$	(0.980 ± 0.005)
Average value	(0.980 ± 0.002)

Table 1. Experimental fidelity of the qubit transfer.

In summary, we have reported the experimental implementation of a device that can transfer a qubit between the orbital angular momentum and polarization degrees of freedom of single photons. The ideal efficiency of the demonstrated device is one, so that the device is theoretically deterministic. The scheme is based on the combination of a q-plate with a Sagnac interferometer containing a Dove prism. While the reported data refer to the OAM to spin qubit transfer only, the same scheme can be used also to implement the inverse process by simply reversing the direction of light propagation in the same setup.

This work was supported by the Future and Emerging Technologies (FET) programme within the Seventh Framework Programme for Research of the European Commission, under FET-Open Grant No. 255914, PHORBITECH. CHM acknowledges the financial support from CNPq (Brazil).

References

1. L. Allen, M. W. Beijersbergen, R. J. C. Spreeuw, and J. P. Woerdman, Phys. Rev. A **45**, 8185 (1992).
2. V. Bazhenov, M. Soskin, and M. Vasnetsov, J. Mod. Opt. **39**, 985 (1992).
3. G. Molina-Terriza, J. P. Torres, and L. Torner, Nature Phys. **3**, 305 (2007).
4. E. Nagali, L. Sansoni, L. Marrucci, E. Santamato, and F. Sciarrino, Phys. Rev. A **81**, 052317 (2010).
5. E. Nagali *et al.*, Phys. Rev. Lett. **105**, 073602 (2010).
6. N. Heckenberg, R. McDuff, C. Smith, and A. White, Opt. Lett **17**, 221 (1992).
7. M. Beijersbergen, L. Allen, H. van der Veen, and J. Woerdman, Opt. Commun. **96**, 123 (1993).
8. M. Beijersbergen, R. Coerwinkel, M. Kristensen, and J. Woerdman, Opt. Commun. **112**, 321 (1994).
9. L. Marrucci, C. Manzo, and D. Paparo, Phys. Rev. Lett. **96**, 163905 (2006).
10. E. Nagali *et al.*, Phys. Rev. Lett. **103**, 013601 (2009).
11. E. Nagali *et al.*, Opt. Express **17**, 18745 (2009).
12. S. Slussarenko, V. D'Ambrosio, B. Piccirillo, L. Marrucci, and E. Santamato, Opt. Express **18**, 27205 (2010).
13. E. Karimi, B. Piccirillo, E. Nagali, L. Marrucci, and E. Santamato, Appl. Phys. Lett. **94**, 231124 (2009).
14. B. Piccirillo, V. D'Ambrosio, S. Slussarenko, L. Marrucci, and E. Santamato, Appl. Phys. Lett. **97**, 241104 (2010).

Experimental Optimal Cloning of Four-Dimensional Quantum States of Photons

E. Nagali,[1] D. Giovannini,[1] L. Marrucci,[2,3] S. Slussarenko,[2] E. Santamato,[2] and F. Sciarrino[1,4,*]

[1]*Dipartimento di Fisica dell'Università "La Sapienza," Roma 00185, Italy*

[2]*Dipartimento di Scienze Fisiche, Università di Napoli "Federico II," Complesso Universitario di Monte S. Angelo, 80126 Napoli, Italy*

[3]*CNR-SPIN, Complesso Universitario di Monte S. Angelo, 80126 Napoli, Italy*

[4]*CNR-Istituto Nazionale di Ottica, Firenze, Italy*

(Received 9 June 2010; revised manuscript received 22 July 2010; published 13 August 2010)

Optimal quantum cloning is the process of making one or more copies of an arbitrary unknown input quantum state with the highest possible fidelity. All reported demonstrations of quantum cloning have so far been limited to copying two-dimensional quantum states, or qubits. We report the experimental realization of the optimal quantum cloning of four-dimensional quantum states, or ququarts, encoded in the polarization and orbital angular momentum degrees of freedom of photons. Our procedure, based on the symmetrization method, is also shown to be generally applicable to quantum states of arbitrarily high dimension—or qudits—and to be scalable to an arbitrary number of copies, in all cases remaining optimal. Furthermore, we report the bosonic coalescence of two single-particle entangled states.

DOI: 10.1103/PhysRevLett.105.073602 PACS numbers: 42.50.Ex, 03.67.−a, 42.50.Dv

Classical information can be freely measured, perfectly copied on demand, and broadcast without fundamental limitations. The handling of quantum information, which is encoded in the quantum states of physical systems, is instead subject to several fundamental restrictions. For example, an unknown quantum state of an individual system cannot be measured completely, unless we have infinite identical copies at our disposal. For a finite number of copies N, the state estimation can only be partial, and it can be characterized by an average "fidelity" lower than one (where one corresponds to perfect state identification). It has been proven that the optimal value of such state-estimation fidelity is given by $F^d_{\mathrm{est}}(N) = (N+1)/(N+d)$, where d is the dimension of the quantum space [1]. A similar restriction is posed by the quantum no-cloning theorem, stating that an unknown quantum state cannot be copied perfectly [2]. It is, however, possible to make imperfect copies, characterized by a cloning fidelity lower than one [3]. Starting with N identical copies of the input state and generating $M > N$ output optimal copies, the optimal copying fidelity is given by $F^d_{\mathrm{clon}}(N,M) = \frac{M-N+N(M+d)}{M(N+d)}$, for the case of "symmetric" cloning, that is, for a uniform fidelity of all copies [4]. It is important to note that, for a given input, the optimal cloning fidelity is always higher than the corresponding optimal state-estimation fidelity, reducing to the latter in the limit $M \to \infty$ [5]. Therefore, the optimal quantum cloning process is useful whenever one needs to broadcast quantum information among several parties without measuring it in the process. Quantum cloning thus represents an important multipurpose tool of the emerging quantum information technology. Let us stress that the advantage of quantum cloning over state estimation grows for an increasing dimension d of the quantum state. More specific applications of quantum cloning are found in the security assessment of quantum cryptography, the realization of minimal disturbance measurements, the enhancement of the transmission fidelity over a lossy quantum channel, and the separation of classical and quantum information [6,7].

It is well known that all tasks of quantum information can be performed by using only two-dimensional quantum states, or qubits. However, it has been recently recognized that significant fundamental and practical advantages can be gained by employing higher-dimensional quantum states instead, or qudits. For example, quantum cryptographic protocols based on qudits may achieve improved security, entangled qudits can show increased resistance to noise, a qudit-based quantum computation may require less resources for its implementation, and the use of quantum computing as physics simulators can be facilitated by using qudits [8–14].

Light quantum states can be used for implementing qudits, either by exploiting many-photon systems [15–17] or by combining different degrees of freedom of the same photon ("hybrid" states) such as linear momentum, arrival time, and orbital angular momentum (OAM) or other transverse modes [18–21]. In particular, we have recently reported the first experimental generation and tomography of hybrid qudits with dimension $d = 4$, also dubbed ququarts, that were encoded in the polarization and OAM of single photons [22].

In this Letter, we report the realization of the optimal quantum cloning $1 \to 2$ (i.e., $N = 1$, $M = 2$) of ququarts ($d = 4$) encoded in the polarization and OAM of single photons. The cloning process is based on the symmetrization technique [23–25] that has been recently proven theoretically to be optimal for arbitrary dimension d [26]. The simultaneous control of polarization and OAM was made

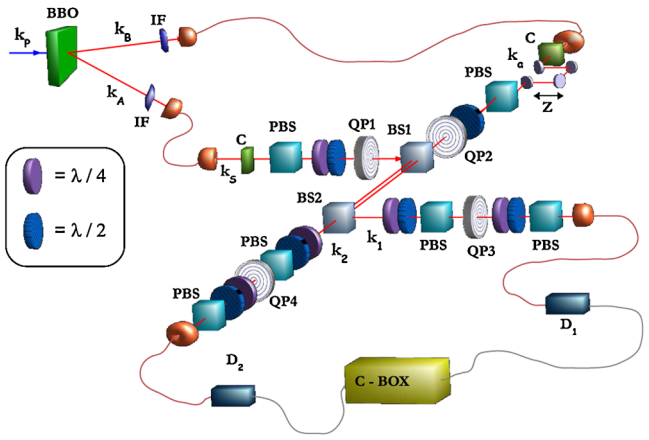

FIG. 1 (color online). Experimental apparatus for implementing the $1 \rightarrow 2$ optimal quantum cloning of polarization-OAM photon ququarts. See the main text for a definition of all symbols.

possible thanks to the q plate, a photonic device introducing a spin-orbit angular momentum coupling [27,28].

Let us recall the working principle of the symmetrization method for $1 \rightarrow 2$ quantum cloning, in the case of a generic d-dimensional quantum state (qudit) [23–26]. The input qudit $|\varphi\rangle_s$ is sent into one input port (mode $\mathbf{k}_s$) of a balanced beam splitter (BS). In the other BS input port (mode $\mathbf{k}_a$) we send an ancilla photon in the fully mixed random d-dimensional state $\rho_a = \frac{\mathrm{I}_d}{d} = \frac{1}{d}\sum_n |n\rangle_a\langle n|$. The basis is here chosen such that $|1\rangle \equiv |\varphi\rangle$. After the interaction in the BS, we consider only the case of the two photons emerging in the same output mode. The cloning fidelity is defined as the average overlap between the quantum state of each output photon emerging from the BS and the input photon state $|\varphi\rangle$. Hence, we can distinguish two cases, depending on the ancilla state: (i) the input state is $|1\rangle_s|1\rangle_a$ or (ii) it is any of the other $d-1$ states $|1\rangle_s|n\rangle_a$ with $n \neq 1$. In the first case, Hong-Ou-Mandel (HOM) quantum interference due to the bosonic symmetry leads to a doubled probability of having the two photons emerging in a common output BS mode, as compared to the second case. So, once given that the two photons emerge in the same mode (i.e., successful cloning occurs), then the first case has a relative probability of $2/(d+1)$ while the second case has a total probability $(d-1)/(d+1)$. Since the first case corresponds to a fidelity of 1 (both photons are identical to the input one) and the second of 0.5 (one photon is identical, and the other is orthogonal), we obtain the following average cloning fidelity: $F = \frac{1}{2} + \frac{1}{d+1}$, which corresponds just to the upper bound for the cloning fidelity $F^d_{\mathrm{clon}}(N, M)$ given above, for $N = 1$ and $M = 2$.

This cloning procedure has been previously demonstrated experimentally only for photonic qubits, encoded either in the polarization space π [24] or in the bidimensional OAM subspace o_2 spanned by $m = \pm 2$ [26], where m is the OAM eigenvalue per photon along the beam axis in units of $\hbar$. We now consider photonic ququarts encoded in the four-dimensional "spin-orbit" space $\pi \otimes o_2$, i.e., obtained as a tensor product of the polarization space and the OAM subspace with $m = \pm 2$. A generic separable state in this space will be indicated as $|\varphi, \ell\rangle = |\varphi\rangle_\pi|\ell\rangle_{o_2}$, where $|\cdot\rangle_\pi$ and $|\cdot\rangle_{o_2}$ stand for the polarization and OAM quantum states, respectively. We introduce in this space a first basis $\{|1_{\mathrm{I}}\rangle, |2_{\mathrm{I}}\rangle, |3_{\mathrm{I}}\rangle, |4_{\mathrm{I}}\rangle\}$, hereafter called the "logic" basis, corresponding to $\{|R, +2\rangle, |R, -2\rangle, |L, +2\rangle, |L, -2\rangle\}$, where R (L) refers to right (left) circular polarization and the ± 2 integers refer to the OAM eigenvalue. Given this first basis, we may introduce four other bases such that they are all *mutually unbiased* to each other [29]. In our spin-orbit space $\pi \otimes o_2$, all the states belonging to the five mutually unbiased basis can be generated and detected by an appropriate combination of birefringent wave plates, polarizing beam splitters, q plates, and single mode fibers, as described in Ref. [22]. Three of these bases (bases I, II, and III) are formed of separable states of polarization and OAM of the photon (e.g., basis I is the logical one defined above), while the remaining two (bases IV and V) are formed of entangled states of these 2 degrees of freedom (see [22] for the complete list of states). In particular, the IV basis, which will be utilized in the present work, is composed of the following four states: $(|R, +2\rangle \pm |L, -2\rangle)/\sqrt{2}$ and $(|L, +2\rangle \pm |R, -2\rangle)/\sqrt{2}$.

We now consider the optimal quantum cloning of a photonic ququart in the spin-orbit space $\pi \otimes o_2$. Because $d = 4$, we expect an optimal cloning fidelity $F = 7/10$. If $|\varphi\rangle = |1\rangle$ is the input state, each output cloned photon (tracing out the state of the other photon) is hence expected to be found in the mixed state:

$$\rho_1 = \rho_2 = \tfrac{1}{10}(7|1\rangle\langle 1| + |2\rangle\langle 2| + |3\rangle\langle 3| + |4\rangle\langle 4|), \quad (1)$$

where the set $\{|1\rangle, |2\rangle, |3\rangle, |4\rangle\}$ forms a basis in the space $\pi \otimes o_2$ (not necessarily the logical one). In particular, we will experimentally test the outcome of the quantum cloning procedure for all four states of the logical basis I and for all four states of the IV basis, corresponding to entangled spin-orbit states.

The experimental layout is schematically reported in Fig. 1. A β-barium borate crystal (BBO) cut for type-II phase matching, pumped by the second harmonic of a Ti:sapphire mode-locked laser beam, generates via spontaneous parametric fluorescence photon pairs on modes k_A and k_B with linear polarization, wavelength $\lambda = 795$ nm, and pulse bandwidth $\Delta\lambda = 4.5$ nm, as determined by two interference filters (IF). The coincidence rate of the source is equal to 18 kHz. Photons generated on mode k_A and k_B are delivered to the setup via single mode fibers, thus defining their transverse spatial modes to a pure TEM_{00}, corresponding to OAM $m = 0$. After the fiber output, two wave plates (C) compensate the polarization rotation introduced by the fibers and a polarizing beam splitter (PBS) projects the polarization on the horizontal state $|H\rangle_\pi$. Then on mode k_s the ququart to be cloned is encoded in the single-photon polarization and OAM through a ququart

preparation stage, based on a combination of wave plates, a q plate, a PBS (only for bases I, II, and III), and additional wave plates (see Ref. [22] for details). On mode k_a, for quantum cloning the ancilla photon is prepared in a fully mixed state $\rho_a = \frac{I_\pi}{2}\frac{I_{o2}}{2}$, i.e., fully randomized both in polarization and in OAM. This is obtained by randomly rotating, during each experimental run, a half-wave plate inserted before the q plate QP2 and by randomly inserting or removing another half-wave plate located after the same q plate. The time delay between photons on mode k_s and k_a was set to zero by an adjustable delay line (Z), in order to ensure the interference condition necessary for the optimal quantum cloning process within the balanced beam splitter BS1. A second beam splitter (BS2) is then used to separate the two photons emerging from the same output port of BS1, allowing postselection of this outcome by coincidence detection. On both output modes k_1 and k_2 of BS2 we perform a full ququart state measurement, by combining a standard polarization analysis set and an OAM analysis set, the latter based on the quantum transferrer $o_2 \rightarrow \pi$ [28]. Depending on the specific ququart basis being used, the detailed setting of this ququart measurement stage varies slightly, as discussed in [22]. Finally, the output photons are coupled into single mode fibers and detected by single-photon counters (D_1 and D_2) connected to the coincidence box (C-BOX) recording the time-coincident photon detections.

As a first step, we have verified the occurrence of the HOM interference between the two photon ququarts impinging on modes k_s and k_a of BS1. The ancillary photon was prepared in the same quantum state as the signal photon, in order for the interference to occur. The two-photon coincidence counts were measured as a function of the optical path delay between k_s and k_a. In Fig. 2(a), we report an example of the results we obtained for the case of an input state belonging to the logical basis. The HOM peak is observed with a measured coincidence enhancement $R = (1.89 \pm 0.05)$, consistent with the theoretical value $R_{\text{th}} = 2$. Once a good interference condition is ensured between the two photons, we moved on to testing the quantum cloning for each of the four input states of the logical basis. $|\varphi\rangle$ being the input state to be cloned, the measurement stage on mode k_1 has been set so as to filter only outcoming photons in state $|\varphi\rangle$, while on mode k_2 all four possible outcomes $|i\rangle$ of the logical basis have been detected. We have thus recorded the corresponding coincidence counts $N_{\varphi,i}$. These coincidence counts give us an estimate of the probability $p(i \mid \varphi)$ of each photon clone to be found in any specific state $|i\rangle$ of the basis, with $i = 1, 2, 3, 4$, as a function of the input state $|\varphi\rangle$, regardless of the state of the other photon. In particular, we have $p(i \mid \varphi) = N_{\varphi,i}/N$ for $i \neq \varphi$ and $p(\varphi \mid \varphi) = (N_{\varphi,\varphi} + \sum_{i\neq\varphi} N_{\varphi,i})/N$, where $N = N_{\varphi,\varphi} + 2\sum_{i\neq\varphi} N_{\varphi,i}$. The factor 2 appearing in the expression of N takes into account the additional coincidences that would be detected by swapping the measurements performed on modes k_1 and k_2, for

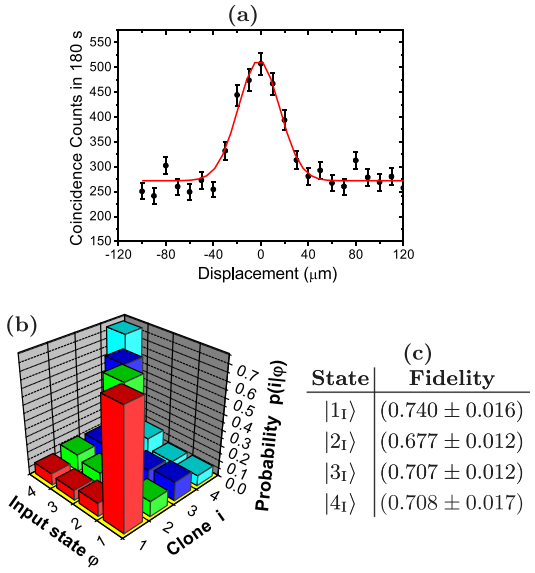

State	Fidelity
$\|1_I\rangle$	(0.740 ± 0.016)
$\|2_I\rangle$	(0.677 ± 0.012)
$\|3_I\rangle$	(0.707 ± 0.012)
$\|4_I\rangle$	(0.708 ± 0.017)

FIG. 2 (color online). Experimental results of the cloning process for the ququart states belonging to the I basis (a) Hong-Ou-Mandel coalescence for two input photons prepared in state $|L, -2\rangle$. The enhancement peak is of $R = (1.89 \pm 0.05)$. (b) Probability $p(i \mid \varphi)$ of detecting a clone in any output state $|i\rangle$ of the basis, for any given input state $|\varphi\rangle$ of the same basis. (c) Experimental cloning fidelities for the four input states.

$i \neq \varphi$, that of course are equal to $N_{\varphi,i}$ in the average. The theoretical values for these probabilities are given by the corresponding coefficients in the clone density matrix in Eq. (1). The cloning fidelity is $F = p(\varphi \mid \varphi)$. The experimental results obtained when cloning all states of the logical basis are reported in Figs. 2(b) and 2(c). The measured values of the fidelity, as well as their average value $\bar{F}_I = (0.708 \pm 0.007)$, are all in good agreement with the theoretical prediction $F = 0.7$.

Cloning only states belonging to the logical basis is clearly not enough to demonstrate the generality of our cloning procedure. We have therefore repeated the cloning experiment for all ququart states belonging to the IV basis, which includes spin-orbit entangled states. These states can be generated and analyzed by exploiting the q-plate capability of entangling and disentangling the polarization and the OAM degree of freedom of a photon. This required removing the first PBS on modes k_1 and k_2 and properly setting the orientation of all wave plates [22]. In Fig. 3, we report the experimental results of the HOM peak for one of the states and of the cloning of all states belonging to the IV basis. Figure 3(a), in particular, demonstrates interference between two single-particle entangled states. As expected, this measurement underlines how the bosonic coalescence of two particles is not tied to the indistinguishability of each individual degree of freedom but rather that of the whole quantum state (whether each of such states is entangled, as is the case in our experiment, or separable). As can be inferred from the table in Fig. 3(c), the cloning

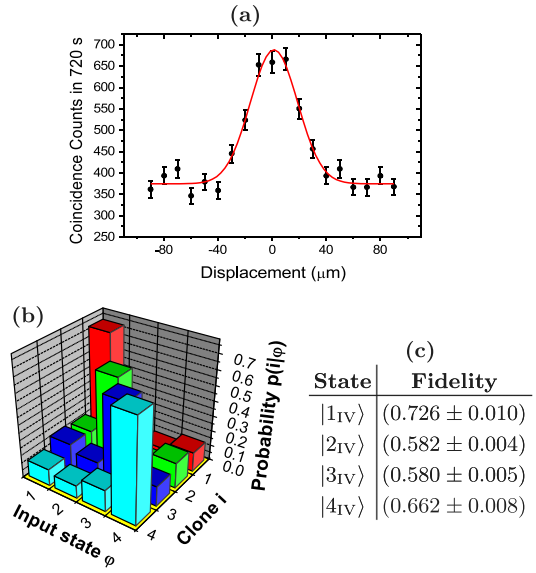

FIG. 3 (color online). Experimental results of the cloning process for all ququart states belonging to the IV basis, made of entangled spin-orbit states. (a) Hong-Ou-Mandel coalescence for two input photons prepared in state $2^{-1/2}(|R,+2\rangle + |L,-2\rangle)$. The enhancement peak is of $R = (1.84 \pm 0.05)$. (b) Probability $p(i \mid \varphi)$ of detecting a clone in an output state $|i\rangle$ of the IV basis, for any given input state $|\varphi\rangle$ of the same IV basis. (c) Experimental cloning fidelities for all four input states.

fidelities are again in reasonable agreement with the expected one, and the average fidelity value reads $\bar{F}_{IV} = (0.638 \pm 0.004)$. The small discrepancy with respect to the theoretical expectations is quantitatively well explained by the imperfect randomization of the ancilla photon (which is found to be somewhat unbalanced), the slightly lower HOM enhancement achieved ($R = 1.84$), and the nonunitary preparation and analysis fidelities ($\sim$0.9) [30]. We stress that the setup alignment has not been reoptimized for cloning states of basis IV, in order to properly test the universality of our cloning apparatus. We notice that the average value of the quantum cloning fidelity is much larger than the one expected for the quantum state estimation on a single copy, equal to 0.4 [5].

Finally, we note that the symmetrization procedure for the cloning of photonic qudits, that we have experimentally demonstrated here for the $1 \rightarrow 2$ case, can be scaled up to the general $N \rightarrow M$ cloning [31], that is, starting with N identical input photons and generating $M > N$ copies. The main idea, illustrated in Fig. 4, is that of using a cascaded

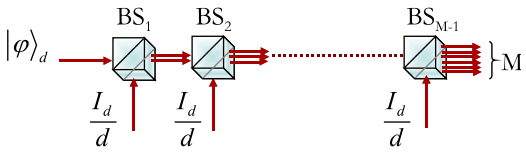

FIG. 4 (color online). Schematic representation of the $1 \rightarrow M$ quantum cloning process of a qudit state by cascading the symmetrization technique.

configuration of $M - N$ beam splitters and $M - N$ ancilla photons in fully mixed states: Fig. 4. A more exhaustive demonstration of this result will be presented in a forthcoming paper.

In summary, we have implemented the optimal quantum cloning $1 \rightarrow 2$ of ququart states encoded in the polarization and OAM degrees of freedom of a single photon.

This work was supported by project HYTEQ—FIRB, Finanziamento Ateneo 2009 of Sapienza Università di Roma, and European project PHORBITECH of the FET program (Grant No. 255914).

*fabio.sciarrino@uniroma1.it

[1] N. Gisin and S. Massar, Phys. Rev. Lett. **79**, 2153 (1997).
[2] W. K. Wootters *et al.*, Nature (London) **299**, 802 (1982).
[3] V. Scarani *et al.*, Rev. Mod. Phys. **77**, 1225 (2005).
[4] P. Navez and N. J. Cerf, Phys. Rev. A **68**, 032313 (2003).
[5] D. Bruß *et al.*, Phys. Lett. A **253**, 249 (1999).
[6] N. Gisin *et al.*, Rev. Mod. Phys. **74**, 145 (2002).
[7] M. Ricci *et al.*, Phys. Rev. Lett. **95**, 090504 (2005).
[8] D. Kaszlikowski *et al.*, Phys. Rev. Lett. **85**, 4418 (2000).
[9] N. J. Cerf *et al.*, Phys. Rev. Lett. **88**, 127902 (2002).
[10] D. Collins *et al.*, Phys. Rev. Lett. **88**, 040404 (2002).
[11] M. Genovese, Phys. Rep. **413**, 319 (2005).
[12] B. P. Lanyon *et al.*, Nature Phys. **5**, 134 (2009).
[13] M. Neeley *et al.*, Science **325**, 722 (2009).
[14] T. Vértesi, S. Pironio, and N. Brunner, Phys. Rev. Lett. **104**, 060401 (2010).
[15] E. V. Moreva *et al.*, Phys. Rev. Lett. **97**, 023602 (2006).
[16] G. Vallone *et al.*, Phys. Rev. A **76**, 012319 (2007).
[17] B. P. Lanyon *et al.*, Phys. Rev. Lett. **100**, 060504 (2008).
[18] J. P. Torres *et al.*, Phys. Rev. A **67**, 052313 (2003).
[19] A. Vaziri *et al.*, Phys. Rev. Lett. **91**, 227902 (2003).
[20] G. Molina-Terriza *et al.*, Phys. Rev. Lett. **92**, 167903 (2004).
[21] N. K. Langford *et al.*, Phys. Rev. Lett. **93**, 053601 (2004).
[22] E. Nagali *et al.*, Phys. Rev. A **81**, 052317 (2010).
[23] M. Ricci *et al.*, Phys. Rev. Lett. **92**, 047901 (2004).
[24] F. Sciarrino *et al.*, Phys. Rev. A **70**, 052305 (2004).
[25] W. T. M. Irvine *et al.*, Phys. Rev. Lett. **92**, 047902 (2004).
[26] E. Nagali *et al.*, Nat. Photon. **3**, 720 (2009).
[27] L. Marrucci, C. Manzo, and D. Paparo, Phys. Rev. Lett. **96**, 163905 (2006).
[28] E. Nagali *et al.*, Phys. Rev. Lett. **103**, 013601 (2009).
[29] A. Klappenecker *et al.*, Lect. Notes Comput. Sci. **2948**, 137 (2004).
[30] The weights of the four components of the ancilla mixed state in the basis IV have been experimentally found to be $w_1 = 0.32$, $w_2 = 0.16$, $w_3 = 0.16$, and $w_4 = 0.36$. By considering the preparation and analysis fidelity and the factor R, we computed the expected fidelity values $F_1 = 0.702$, $F_2 = 0.594$, $F_3 = 0.597$, and $F_4 = 0.68$, with mean value $F_{IV} = 0.645$, in good agreement with the experimental results.
[31] L. Masullo, M. Ricci, and F. DeMartini, Phys. Rev. A **72**, 060304 (2005).